www.sciencemag.org/cgi/content/full/1165395/DC1

Supporting Online Material for

Genomic Loss of microRNA-101 Leads to Overexpression of Histone Methyltransferase EZH2 in Cancer

Sooryanarayana Varambally, Qi Cao, Ram-Shankar Mani, Sunita Shankar, Xiaosong Wang, Bushra Ateeq, Bharathi Laxman, Xuhong Cao, Xiaojun Jing, Kalpana Ramnarayanan, J. Chad Brenner, Jindan Yu, Jung H. Kim, Bo Han, Patrick Tan, Chandan Kumar-Sinha, Robert J. Lonigro, Nallasivam Palanisamy, Christopher A. Maher, Arul M. Chinnaiyan*

*To whom correspondence should be addressed. E-mail: arul@umich.edu

Published 13 November 2008 on *Science* Express
DOI: 10.1126/science.1165395

This PDF file includes:

SUPPORTING ONLINE MATERIAL

Genomic Loss of microRNA-101 Leads to Overexpression of Histone Methyltransferase EZH2 in Cancer

Sooryanarayana Varambally,[1,3,6,*] Qi Cao,[1,3,*] Ram-Shankar Mani,[1,3] Sunita Shankar,[1,3] Xiaosong Wang,[1,3] Bushra Ateeq,[1,3] Bharathi Laxman,[1,3] Xuhong Cao,[1,2] Xiaojun Jing,[1,3] Kalpana Ramnarayanan,[7] J. Chad Brenner,[1,3,5] Jindan Yu,[1,3] Jung H. Kim,[1,3] Bo Han,[1,3] Patrick Tan,[7,8] Chandan Kumar-Sinha,[1,3] Robert J. Lonigro,[1,6] Nallasivam Palanisamy,[1,3,7] Christopher A. Maher,[1,3] and Arul M. Chinnaiyan[1,2,3,4,5,6,#]

[1]Michigan Center for Translational Pathology, [2]Howard Hughes Medical Institute, [3]Department of Pathology, [4]Urology, [5]Cellular and Molecular Biology, and the [6]Comprehensive Cancer Center University of Michigan Medical School, Ann Arbor, MI 48109, USA
[7]National Cancer Centre, Singapore and the [8]Genome Institute of Singapore

* These authors contributed equally

[#]Address correspondence and requests for reprints to:
Arul M. Chinnaiyan, M.D., Ph.D.

This PDF contains:

Materials and Methods

microRNA Prediction Tools

To identify miRNAs targeting *EZH2*, we integrated the output results of multiple prediction programs; TargetScan [http://www.targetscan.org/] (*1*), PicTar [http://pictar.org/] (*2*), miRanda [http://www.microrna.org/microrna/](*3*), and miRInspector [http://mirna.imbb.forth.gr/microinspector/] *(4)*. Each program was selected to leverage the various strengths for predicting miRNA targets in the areas of sequence alignment, thermodynamics, and comparative genomics. TargetScan requires a perfect seed, a sub-region of alignment between the miRNA and mRNA, while incorporating traditional RNA folding calculations and conservation of the binding site across vertebrates. PicTar, while preferring a perfect seed match, tolerates imperfect seed matches when they simultaneously adhere to heuristically defined thermodynamic requirements. miRanda employs a dynamic programming algorithm to establish miRNA:mRNA sequence alignment in addition to thermodynamics and conservation across multiple species. Lastly, microInspector identifies possible binding sites within an mRNA sequence relying heavily on free energy values at a binding site. We developed a Perl script that imported the various output formats from each of the target prediction programs and subsequently integrated the results to detect common overlaps. For instance where all programs report an miRNA:mRNA interaction, the candidate miRNAs are sorted based on the predefined rankings from each respective program. Additionally, we export the number of predicted binding sites for miR-101 in the *EZH2* 3'UTR.

Cell Lines

Breast cancer cell line SKBr3 were grown in RPMI 1640 (Invitrogen, Carlsbad, CA) with 10% FBS (Invitrogen) in 5% CO_2 cell culture incubator, and prostate cancer cell line DU145 were grown in MEM with 10% FBS in 5% CO_2 cell culture incubator. Immortalized breast cell lines HME and H16N2 were grown in F-12 Nutrient Mixture with 5ug/ml Insulin (Sigma,), 1ug/ml Hydrocortisone(Sigma), 10ng/ml EGF (Invitrogen), 5mM Ethanolamine (Sigma) , 5ug/ml Transferrin (Sigma), 10nM Triiodo Thyronine (Sigma), 50nM Sodium Selenite (Sigma), 10mM HEPES (Invitrogen) and 50 unit/ml Penstrep (Invitrogen), 10% CO_2. For mir-101 overexpression, pMIF-cGFP-Zeo construct expressing mir-101 was obtained from System Biosciences (Mountain View, CA). Lentiviruses were generated by the University of Michigan Vector Core. Prostate cancer cell line DU145 and breast cancer cell line SKBR3 were infected with lentiviruses expressing mir-101 or vector only, and stable cell lines were generated by selection with 300 ug/ml zeocin (Invitrogen, Carlsbad, CA). To generate stable EZH2 knockdown, shRNA lentiviral particles for EZH2 gene silencing and control vector were obtained from Sigma-Aldrich (St. Louis, MO). Prostate cancer cell line DU145 was infected with EZH2 shRNA lentivirus and a stable cell line was generated by selection with 1 ug/ml Puromycin (Sigma-Aldrich, St. Louis, MO).

Tissues

In this study we utilized tissues from clinically localized prostate cancer patients, who underwent radical prostatectomy as a primary therapy between 2004-2006 at the University of Michigan Hospital, androgen-independent metastatic prostate cancer patients from a rapid autopsy program described previously (*5, 6*), and patients with invasive carcinomas of the breast. The detailed clinical and pathological data were maintained on a secure relational database. This study was approved by the Institutional Review Board at the University of Michigan Medical School. Both radical prostatectomy

series and the rapid autopsy program were part of the University of Michigan Prostate Cancer Specialized Program of Research Excellence Tissue Core. Breast cancer tissues were collected with IRB approval from the University of Singapore/National University Hospital, Singapore (NUS/NUH). The gastric cancer samples were collected with IRB approval from the National Cancer Center, Singapore.

microRNA Transfection, AntagomiR transfection, and small RNA interference

Knockdown of EZH2 was accomplished by RNA interference using siRNA duplex (Dharmacon, Lafayette, CO) as previously described (*7*). Precursors of respective microRNAs and negative controls used in this study were purchased from Ambion (Austin, TX). AntagomiR-101 and negative control antagomiRs were purchased from Dharmacon. Transfections were performed with oligofectamine or lipofectamine (Invitrogen) depending on the cell line used.

miR Reporter Luciferase Assays

The 3'UTR (untranslated region) or the antisense sequence of the 3'UTR of *EZH2* as well as mutant 3'UTR of *EZH2* were cloned into the pMIR-REPORT™ miRNA Expression Reporter Vector (Ambion). SKBr3 cells were transfected with pre-miR-101 or controls and then co-transfected with 3'-UTR-luc or mutant 3'UTR-luc, as well as pRL-TK vector as internal control for luciferase activity. Post 48 hours of incubation, the cells were lysed and luciferase assays conducted using the dual luciferase assay system (Promega, Madison, WI). Each experiment was performed in triplicate.

Quantitative Real-Time PCR Assays

Total RNA was isolated from SKBr3 and DU145 cells that were transfected either with pre-miR-101, or control precursors (Qiagen). Quantitative PCR (QPCR) was performed using SYBR Green dye on an Applied Biosystems 7300 Real Time PCR system (Applied Biosystems, Foster City, CA) as described (*5*). Briefly, 1 μg of total RNA was reverse transcribed into cDNA using SuperScript III (Invitrogen, Carlsbad, CA) in the presence of random hexamers and oligo dT primers (Invitrogen). All reactions were performed in triplicate with SYBR Green Master Mix (Applied Biosystems) plus 25 ng of both the forward and reverse primer according to the manufacturer's recommended thermocycling conditions, and then subjected to melt curve analysis. Threshold levels for each experiment were set during the exponential phase of the QPCR reaction using Sequence Detection Software version 1.2.2 (Applied Biosystems). The DNA in each sample was quantified by interpolation of its threshold cycle (C_t) value from a standard curve of C_t values, which were created from a serially diluted cDNA mixture of all samples. The calculated quantity of the target gene for each sample was divided by the average sample quantity of the housekeeping genes, glyceraldehyde-3-phosphate dehydrogenase (*GAPDH*) to obtain the relative gene expression. All oligonucleotide primers were synthesized by Integrated DNA Technologies (Coralville, IA). The primer sequences for the transcript analyzed are provided in **table S4**.

For microRNA quantitative PCR, total RNA including small RNA was isolated from prostate tissues, SKBr3 and DU145 cells that were transfected either with pre-hsa-miR-101 (precursor human miRNA-101), or control precursors. Total RNA was used at 10ng/ul. For RT, master mix were prepared using 0.15ul 100mM dNTPs, 1.00ul MultiScrible Reverse Transcriptase (50U/ul), 1.50ul 10X Reverse

Transcription Buffer, 0.188ul RNase Inhibitor (20U/ul) and 4.192ul Nuclease-free water. Each 15ul RT reaction mix contained, 7ul of master mix, 5ul of RNA samples (10ng/ul) and 3ul 5X specific RT primer. Thermal cycler was programmed as follows: 16 degrees for 30 minutes, 42 degrees for 30 minutes and 85 degrees for 5 minutes. Each PCR reaction mix contained 10 ul of Taqman 2X Universal PCR Master Mix (No AmpErase UNG), 6.67ul Nuclease-free water, 1ul 20X specific PCR primer and 1.33ul RT product. Thermal cycler was programmed as follows: 95 degrees for 10 minutes, 40 cycles of 95 degrees for 15seconds and 60 degrees for 60seconds. Using the comparative CT method, we used endogenous control (RNU6B) to normalize the expression levels of target micro-RNA by correcting differences in the amount of RNA loaded into qPCR reactions.

Genomic PCR Assays

Genomic DNA from benign (n=15), localized prostate cancer (n=16) and metastatic (n=33) prostate cancer tissues were isolated. DNA from benign (n=7), tumor (n=29) and metastatic (n=1, three different sites) from breast cancer cases were also isolated. For genomic analyses of the miR-101 loci, the 2^-ΔΔCt method was adapted using SyBr green based quantitative PCR (qPCR) (*8, 9*). Briefly, 100ng 25ng of gDNA was used as template to amplify the miR-101-1, miR-101-2 and miR-217 encompassing loci. Since miR-217 levels did not show significant correlation with *EZH2* transcript levels, miR-217 was used as the reference for relative quantification. The assay was validated using the methods described (*8, 9*). For unification of data and to avoid inter-assay differences Ct values for the reference gene (miR-217) were always estimated simultaneously with miR-101-1 or miR-101-2. A representative benign tissue sample was used in every assay as a calibrator sample to which every sample was compared, to obtain a relative quantitation (RQ) value. To calibrate the extent of loss in the miR-101 loci we determined the relative levels of 9 different genomic regions on X-chromosome (three regions in phosphoglycerate kinase 1 (PGK1) gene, and six X-chromosome specific miRNAs- miR-424, miR-503, miR-766, miR-448, miR-222 and miR-221) in the genomic DNA from a normal male sample (1X) as compared to a normal female sample (2X) genomic DNA (Promega) that are located only on the X chromosome. RQ values for these regions in male genomic DNA were assessed using a non-X-chromosome gene Tata Binding Protein (TBP) gene as the reference gene (9). An RQ value of 0.7 and below was considered as loss of at least one copy of the genomic loci (**Table S5**), similar to earlier reports(*8, 9*). Accordingly, samples showing values lower than 0.7 were considered to have a hemizygous loss and those below 0.3 were considered to exhibit a homozygous loss. For the loss of heterozygosity (LOH) analysis, 9 cancer samples showing miR-101-1 deletion were identified and normal (non prostatic) tissues from the same cases were obtained. Genomic qPCR analysis was carried out in these as described above and RQ values obtained were compared to those obtained from the matched cancer cases. Primer sequences used for genomic PCR assays are given in **Table S6.**

Immunoblot Analyses

The breast cancer cell lines SKBr3 and prostate cancer cell DU145 were transfected with pre-miR-101 or controls. The breast cell lines H16N2 and HME were transfected with antagomiR-101 or negative controls. Post 72 hours transfection, cells were homogenized in NP40 lysis buffer (50 mM Tris-HCl, 1% NP40, pH 7.4, Sigma, St. Louis, MO), and complete proteinase inhibitor mixture (Roche, Indianapolis, IN). Ten micrograms of each protein extract were boiled in sample buffer, separated by SDS-PAGE, and transferred onto Polyvinylidene Difluoride membrane (GE Healthcare, Piscataway, NJ). The membrane was incubated for one hour in blocking buffer [Tris-buffered saline, 0.1% Tween (TBS-T), 5% nonfat

dry milk] and incubated overnight at 4ºC with the following: anti-EZH2 mouse monoclonal (1:1000 in blocking buffer, BD Biosciences Cat # 612667, San Jose, CA), anti-EED rabbit polyclonal (1:1000, Santa Cruz Biotech, Cat #: sc-28701, Santa Cruz, CA), anti-SUZ12 mouse monoclonal (1:1000, Upstate, Cat #: 04-046, Charlottesville, VA), and anti-N-myc rabbit polyclonal antibodies (1:1000, Cell Signaling Tech, Cat #: 9405, Danvers, MA), anti-ARID1A mouse monoclonal antibody (1:1000, Abcam, Cat #: ab50878, Cambridge, MA), anti-FBN2 rabbit polyclonal antibody (1:1000, Abcam, Cat #: ab21619), anti-c-Fos mouse monoclonal antibody (1:1000, BD Biosciences, Cat #: 554156), anti-trimethyl-H3K27 rabbit polyclonal (1:2000, Upstate, Cat #: 07-449), anti-monomethyl-Histone H3 (Lys27) (1:1000 upstate Cat #: 07-448), anti-acetyl-Histone H3 (K27) (upstate Cat #: 07-360) and anti-total Histone H3 rabbit polyclonal (1:5000, Cell Signaling, Cat #: 9715) and anti-GAPDH mouse monoclonal antibody (1:10000, Abcam, Cat #: ab9482). Following a wash with TBS-T, the blot was incubated with horseradish peroxidase-conjugated secondary antibody and the signals visualized by enhanced chemiluminescence system as described by the manufacturer (GE Healthcare).

Cell Proliferation Assay

Cells were plated in 24-well plates at desired cell concentration and transfected with precursor microRNA or controls. Cell counts were estimated by trypsinizing cells and analysis by Coulter counter (Beckman Coulter, Fullerton, CA) at the indicated time points in triplicate.

Cell Migration Assay Using Wound Healing Assay

DU145 lenti-vector and miR-101 overexpressing, and sh-vector and EZH2 knockdown stable cells were grown to confluence. An artificial wound was created using a 1ml pipette tip on confluent cell monolayer. To visualize migrated cells and wound healing, cell images were taken at 0, 24, 48 and 72hrs.

Basement Membrane Matrix Invasion Assays

For invasion assays, the breast cell lines H16N2 and HME were transfected with antagomiR-101 or negative controls. Invasive breast cancer cell SKBr3 and prostate cancer cell DU145 were transfected with pre-miR-101 or controls. Forty-eight hours post-transfection, cells were seeded onto the basement membrane matrix (EC matrix, Chemicon, Temecula, CA) present in the insert of a 24 well culture plate. Fetal bovine serum was added to the lower chamber as a chemoattractant. After 48 hours, the non-invading cells and EC matrix were gently removed with a cotton swab. Invasive cells located on the lower side of the chamber were stained with crystal violet, air dried and photographed. For colorimetric assays, the inserts were treated with 150 µl of 10% acetic acid and the absorbance measured at 560nm using a spectrophotometer (GE Healthcare).

Soft Agar Colony Formation Assays

A 50µL base layer of agar (0.6% Agar in DMEM with 10% FBS) was allowed to solidify in a 96-well flat-bottom plate prior to the addition of a 75µL wild type DU145, DU145 miR-101 clones or vector transfected DU145 cell suspension containing 4,000 cells in 0.4% Agar in DMEM with 10% FBS. The cell containing layer was then solidified at 4C for 15 minutes prior to the addition of 100µL of MEM with 5% FBS. Colonies were allowed to grow for 21 days before imaging under a light microscope.

Prostate Tumor Xenograft Model

All procedures involving mice were approved by the University Committee on Use and Care of Animals (UCUCA) at the University of Michigan and conform to their relevant regulatory standards. Five-week-old male nude athymic BALB/c nu/nu mice (Charles River Laboratory, Wilmington, MA) were used for examining the tumorigenicity. To evaluate the role of miR-101 overexpression in tumor formation, the DU145 stable cells overexpressing miR-101 or vector control cells were propagated and $5x10^6$ cells were inoculated subcutaneously into the dorsal flank of ten mice (n = 5 per group). Tumor size was measured every week, and tumor volumes were estimated using the formula $(\pi/6)$ $(L \times W^2)$, where L = length of tumor and W = width.

Chromatin Immunoprecipitation (ChIP) Assays

The effect of miR-101 over-expression on trimethyl H3 (Lys-27) status of EZH2 targets was determined by Chromatin Immunoprecipitation (ChIP) assay. The ChIP assay was carried out with antibodies against trimethyl H3 (Lys-27) (Mouse monoclonal from Abcam, Cat: Ab6002-100). The assay was performed using the EZ-Magna ChIP kit (Millipore) according to the manufacturer's protocol. Briefly, 2×10^6 cells were used for each immunoprecipitation. The cells were cross-linked for 10 minutes by addition of formaldehyde to a final concentration of 1 %. The cross-linking was stopped by 1/20V of 2.5M glycine. This was followed by cell lysis and sonication, resulting in an average fragment size of 500 bp. Antibody incubations were carried out over-night at 4°C. Reversal of cross-linking was carried out at 65°C for 3 hours, followed by DNA isolation. The purified DNA was analyzed by quantitative PCR to determine fold enrichment relative to input DNA. The primer sequences for the promoters analyzed are provided in **Table S7**.

Gene Expression Profiling

Expression profiling was performed using the Agilent Whole Human Genome Oligo Microarray (Santa Clara, CA) according to the manufacturer's protocol. SKBr3 cells were transfected with pre-miR-101 or negative control for precursor microRNA. Over- and under-expressed signatures were generated by filtering to include only features with significant differential expression (Log ratio, $P < .01$) in all hybridizations and two-fold average over- or under-expression (Log ratio) after correction for the dye flip. To ensure that we were comparing robust gene expression alterations, we analyzed biological replicates and used only the probes showing expression changes in both replicates.

Array Comparative Genomic Hybridization

Comparative genomic hybridization analysis for prostate, breast and gastric cancers were carried using oligonucleotide based comparative genomic hybridization array (Hg17 genome build) (Agilent Technologies, USA) according the manufacture's instructions. Competitive hybridization of differentially labeled tumor and reference DNA to oligonucleotide printed in an array format and analysis of fluorescent intensity for each probe will detect the copy number changes in the tumor sample relative to normal reference genome. We analyzed copy number changes for miR-101-1 (1p31.3) and miR-101-2 (9p24.1) regions with a change in copy number level of at least one copy (log ratio ± 0.5) for

losses involving more than one probe representing each genomic interval as detected by the aberration detection method (ADM-2) in CGH analytics software 3.5 (Agilent Technologies) algorithm.

Analysis of Publicly Available Array CGH/SNP Datasets for miR-101 Copy Number Analysis

To examine the mir-101 loss status in multiple cancers, we collected the public array CGH/SNP datasets from Gene Expression Omnibus (http://www.ncbi.nih.gov/geo) and Cancer Bioinformatics Grid (https://cabig.nci.nih.gov/). Acute lymphoblastic leukemia (*10*), glioblastoma (Data from TCGA) and lung cancer (*11*) studies were analysed. The sample information was manually curated and classified into cancer (primary plus metastasis), metastasis and normal samples.

For the Affymetrix SNP arrays, model-based expression was performed to summarize signal intensities for each probe set, using the perfect-match/mismatch (PM/MM) model. For copy number inference, raw copy number was calculated by comparing the signal intensity of each SNP probe set for each tumor sample against a diploid reference set of samples. All of the resulting DNA copy number ratios were transformed by log 2. In the two-channel array CGH datasets, the differential ratio between the processed testing channel signal and processed reference channel signal were calculated and transformed by log 2, which reflects the DNA copy number difference between the testing channel and reference channel.

In the normalization step, the log ratios were transformed into a normal distribution with a mean of 0 under the null model assumption. The data were segmented by circular binary segmentation (CBS) algorithm developed by Olshen et al, (*12*) a method for identifying all genomic change points where the mean log ratio score changes between intervals. The threshold for deletion was modified from the report by Mullighan et al, (*10*). Cutoffs of 0.9 and 0.3 were used to identify hemizygous and homozygous deletions, respectively. The probe closest to the selected gene was used to represent the DNA copy number status of this gene, with a maximal distance of 10kb.

Statistical Analyses

All gene expression and relative quantification data were analyzed on the log (base 2) scale. Comparisons between gene expression values across sample classes were made using two-sample Student's t-test. The significance of associations between EZH2 and miR-101 expression values was judged via a test statistic based on Pearson's product moment correlation coefficient. Associations between binary variables (loss at the two miR-101 loci, and overlap of gene sets) were explored using Fisher's exact test. The relationship between EZH2 overexpression and miR-101 loss was evaluated using a test statistic calculated as the minimum observed value of EZH2 expression in the set of samples exhibiting miR-101 loss at either locus. The null permutation distribution of this statistic was derived by randomly permuting miR-101 loss status within the set of samples; N=10000 permutations were used.

The significance of the separation between miR-101 and vector trajectories in the mouse xenograft model was evaluated via a linear mixed model that incorporated a random intercept for each mouse and used square-root transformed tumor volume measurements as dependent variable. Wald tests were used

to assess the statistical significance of observed differences between growth rates in the two groups of mice.

All statistical tests were two-sided and constructed at the $\alpha=0.05$ significance level except for the above-described permutation test, which was one-sided and conducted at the $\alpha=0.025$ significance level. Statistical analyses were performed using R, version 2.7.0 (http://www.r-project.org).

Supplementary Results and Discussion

To extend our findings of miR-101 deletion to other solid tumors, we first examined breast cancers and found that 6 of 29 breast cancers exhibited loss of miR-101-1 (**fig. S17**). We had a single breast cancer metastasis, and interestingly, all 3 samples from this patient had marked copy number loss in the miR-101-1 locus. Genomic PCR of the miR-101-2 locus did not produce a significant number of breast cancers exhibiting loss. As EZH2 has been shown to be elevated in a wide variety of cancers (*7, 13-19*), we examined whether miR-101 genomic loss was similarly prevalent across cancer types. In addition, we wanted to complement our genomic PCR assessments with other approaches to measure copy number loss (i.e., array CGH and Affymetrix SNP arrays). We compiled Agilent array CGH data for the region flanking the miR-101 from prostate, breast, and gastric cancer from our group ((**tables S8-10 and fig. S15, 16**). In our prostate cancer Agilent array CGH dataset 22.7% (18/79) tumors exhibited complete loss or loss of heterozygosity of the miR-101 locus and 48.5% (16/33) of metastatic disease showed genomic loss of miR-101. Agilent breast cancer array CGH dataset (n=40), showed 60% of cancers with miR-101 loss, either complete deletion of loss of heterozygosity. Gastric cancer array CGH data indicated 56.2% (36/64) cases with miR-101 loss.

Furthermore, we interrogated published data and publicly available data from The Cancer Genome Anatomy (TCGA) project. Examining the glioblastoma multiforme dataset (n=145) from the TCGA it was observed that 18.7% of cases exhibit loss of miR-101. In a lung adenocarcinoma dataset (*11*) by Zhao et al (n=63), 37.3% of the cases exhibited loss of the miR-101.

Of note, one of the most extensive studies represented in our meta-analysis (based on genomic coverage and number of patients) was by Mullighan et al, (*10*) which used 500K Affymetrix SNP arrays to study aberrations in 369 acute lymphoblastic leukemias (ALL) and controls. Of these, 127 were matched samples representing the active phase of disease (cancer) and remission phase ("normal"). Interestingly, 15.3% of the active phase samples exhibited loss of the miR-101-2 locus (and only 1.2% exhibited loss of miR-101-1) (**fig. S18**). None of the matched controls (remission phase samples) displayed loss in either of the genomic loci confirming the somatic nature of this aberration. Furthermore, it is interesting to note that miR-101-2 loss does not occur frequently in the TEL-AML sub-type of ALL (**fig. S18**) the biological implications of which are unclear.

Overall, this study began with a search for miRNAs that might regulate EZH2 expression, an important mediator of epigenetic pathways in embryonic stem cells and malignant progression. While several miRNA candidates were nominated by computational algorithms, we show that experimentally only miR-101 directly regulates EZH2 expression and is inversely associated with EZH2 levels in cancer progression. miR-101 has properties consistent with that of a tumor suppressor gene that functions by negatively regulating the oncogenic potential of EZH2. Furthermore, miR-101, by virtue of its regulation of EZH2, may have profound control over the epigenetic pathways active not only in cancer cells, but in normal pluripotent embryonic stem cells. We demonstrated that overexpression of miR-101 decreases the level of trimethyled histone H3K27 in cancer cells and presumably can configure the histone code of cancer cells to more of a benign phenotype. Presumably miR-101 is a functional regulator of the PRC2 complex and is expressed at high levels in differentiated cells and at low levels in embryonic stem cells and subsets of more aggressive cancers leading to EZH2 and PRC2 induction. Importantly, we discovered a genetic mechanism for EZH2 elevation in cancer that involves the somatic

loss of the miR-101 genomic loci. Similar to EZH2 being broadly elevated in subsets of cancers, our meta-analysis revealed that the miR-101 genomic loci is lost in a subset of different cancer types. As the loss of miR-101 and concomitant elevation of EZH2 is most pronounced in metastatic cancer, we postulate that miR-101 loss may represent a progressive molecular lesion in the development of more aggressive disease. Approaches to re-introduce miR-101 into tumors may have therapeutic benefit by reverting the epigenetic program of tumor cells to a more normal state.

Supplementary Figures

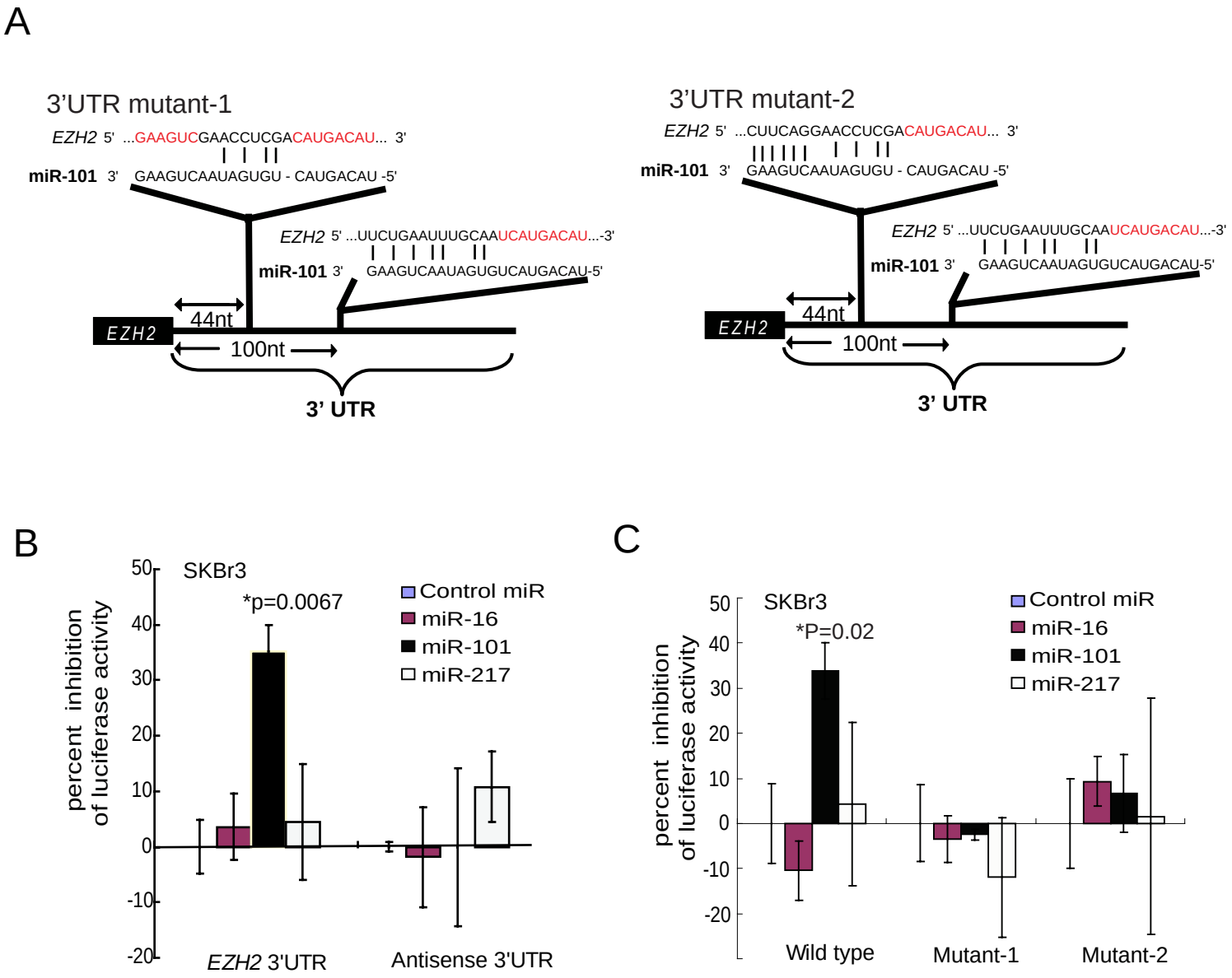

Figure S1. miR-101 regulation of the 3'UTR of EZH2. (**A**) Schematic of mutant EZH2 3'UTRs that were created. Red nucleotides represent regions that were altered to affect potential miR binding. (**B**) SKBr3 breast carcinoma cells were co-transfected with miR-101, control miR, miR-16 or miR-217 together with a reporter vector containing firefly luciferase linked to the 3'UTR of EZH2 (see supplementary methods for details). Percent inhibition of bioluminescence was quantitated. S.E.M. of 3 replicates. The p-value was calculated between control miR and miR-101. (**C**) Same as in B, but instead of antisense, mutant 3'UTR reporters of EZH2 were used as controls.

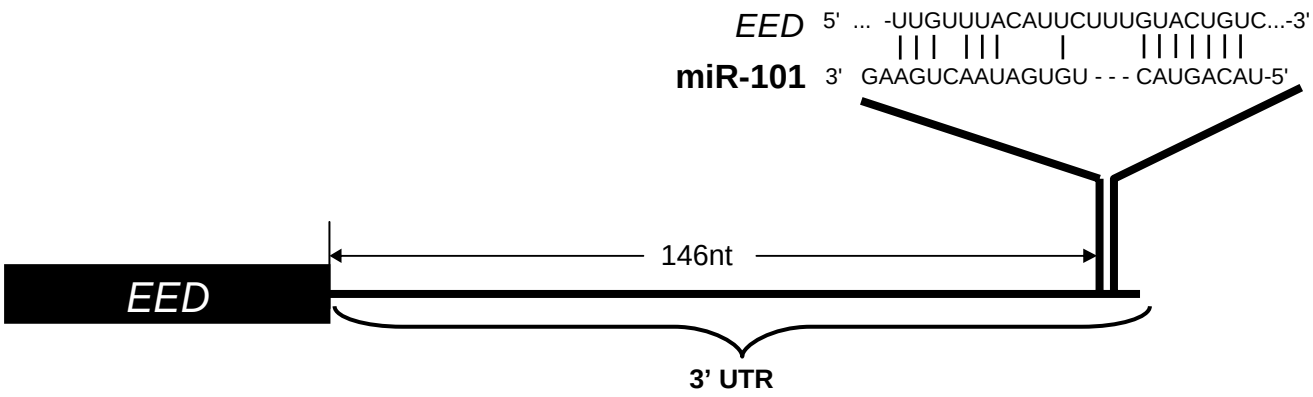

Figure S2. Schematic of predicted miR-101 binding site in the EED 3'UTR

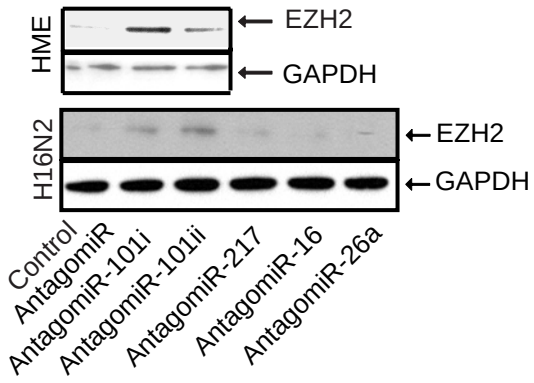

Figure S3. AntagomiRs of miR-101 induce EZH2 protein expression. Top panel, immortalized human mammary epithelial (HME) cells transfected with two independent antagomiRs targeting miR-101 (i and ii). Bottom panel, as above, but immortalized H16N2 benign mammary epithelial cells. Control antagomiR and antagomiR-217, -16 and -26a were also used. Immunoblot was performed using EZH2 antibody and blot was re-probed with GAPDH antibody. Representative experiments are shown.

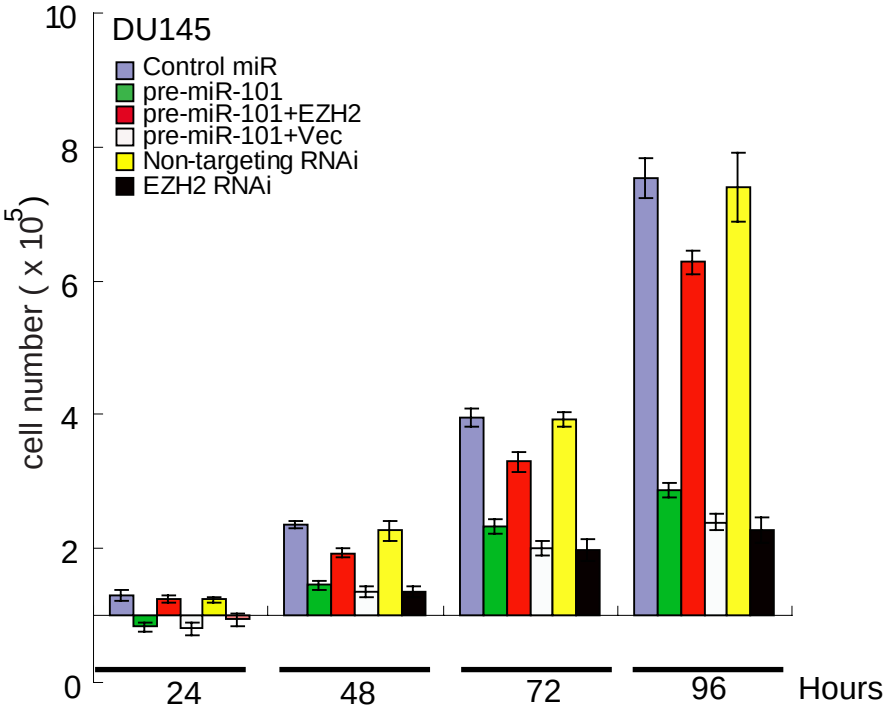

Figure S4. miR-101 overexpression reduces cell proliferation. Cell growth assay of DU145 cells treated with either precursor miR-101 or siRNA targeting EZH2. Cell growth relative to the control miRNA and control siRNA duplex was measured. Rescue experiments were performed by overexpressing EZH2 in miR-101-treated cells.

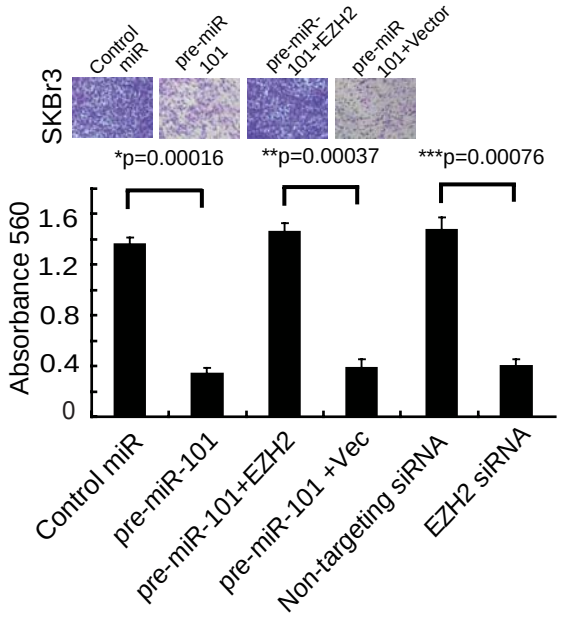

Figure S5. miR-101 expression decreases cell invasion of SKBr3 breast carcinoma cells. Cells were transfected with miR-101 or EZH2 specific siRNA, control miR and non-targeting siRNA. miR-101 was also overexpressed in those cells overexpressing EZH2 by andenoviral infection. All cells were subjected to a matrigel invasion assay. Representative fields of invaded and stained cells are shown in upper panel

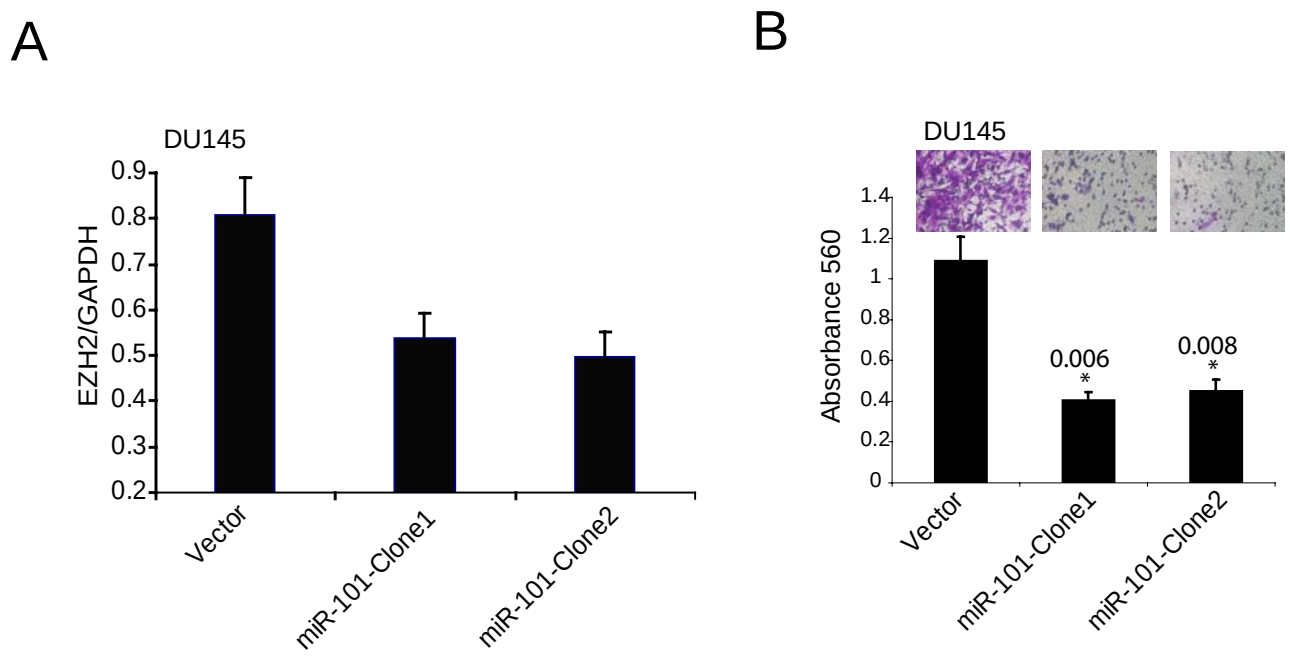

Figure S6. DU145 stable cells overexpressing miR-101 express lower levels of EZH2 and reduces invasion. (**A**). QRT-PCR analysis of DU145 cell clones stably transfected with miR-101. (**B**). Reconstituted basement membrane invasion chamber assay of DU145 cell clones stably transfected with miR-101. Representative fields of invaded and stained cells are shown.

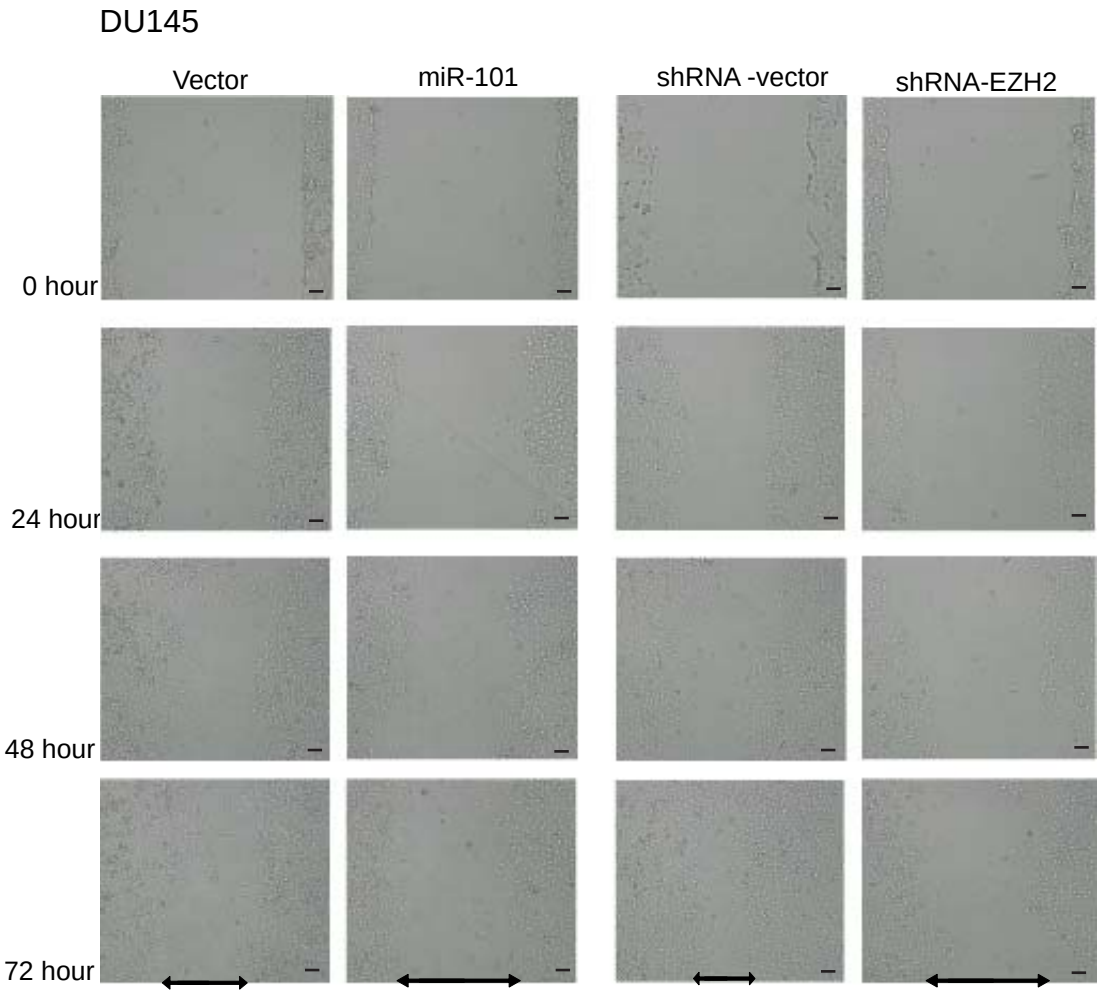

Figure S7. miR-101 overexpression and EZH2 knockdown markedly decrease cell motility in DU145 prostate cancer cells as measured by scratch assay. An artificial wound was created using a 1 ml pipette on a confluent monolayer of cells. Images were taken at 0, 24, 48, and 72 hrs after wound.

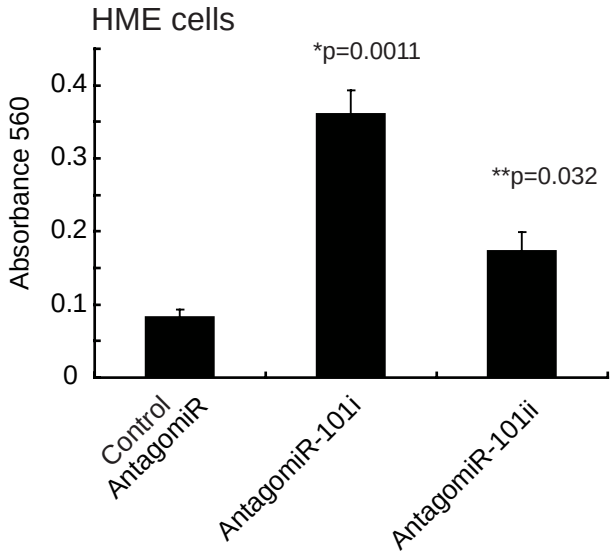

Figure S8. AntagomiRs to miR-101 induce the invasiveness of benign immortalized HME breast epithelial cells. Control antagomiR was used in the assay and the treated cells were used in invasion assays. p-values were calculated between control antagomiR and antagomiR-101 i or antogomiR-101 ii (each representing independent antagomiRs).

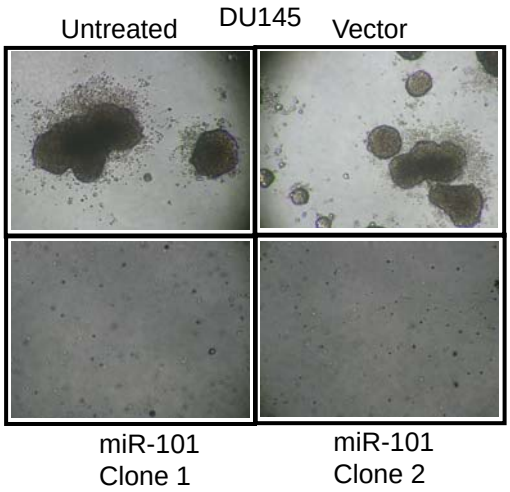

Figure S9. miR-101 over-expression blocks the anchorage-independent growth of cancer cells. DU145 prostate cancer cells were stably transfected with miR-101 or control plasmid and assayed for soft agar colony formation. Untreated and vector stable lines were used as controls.

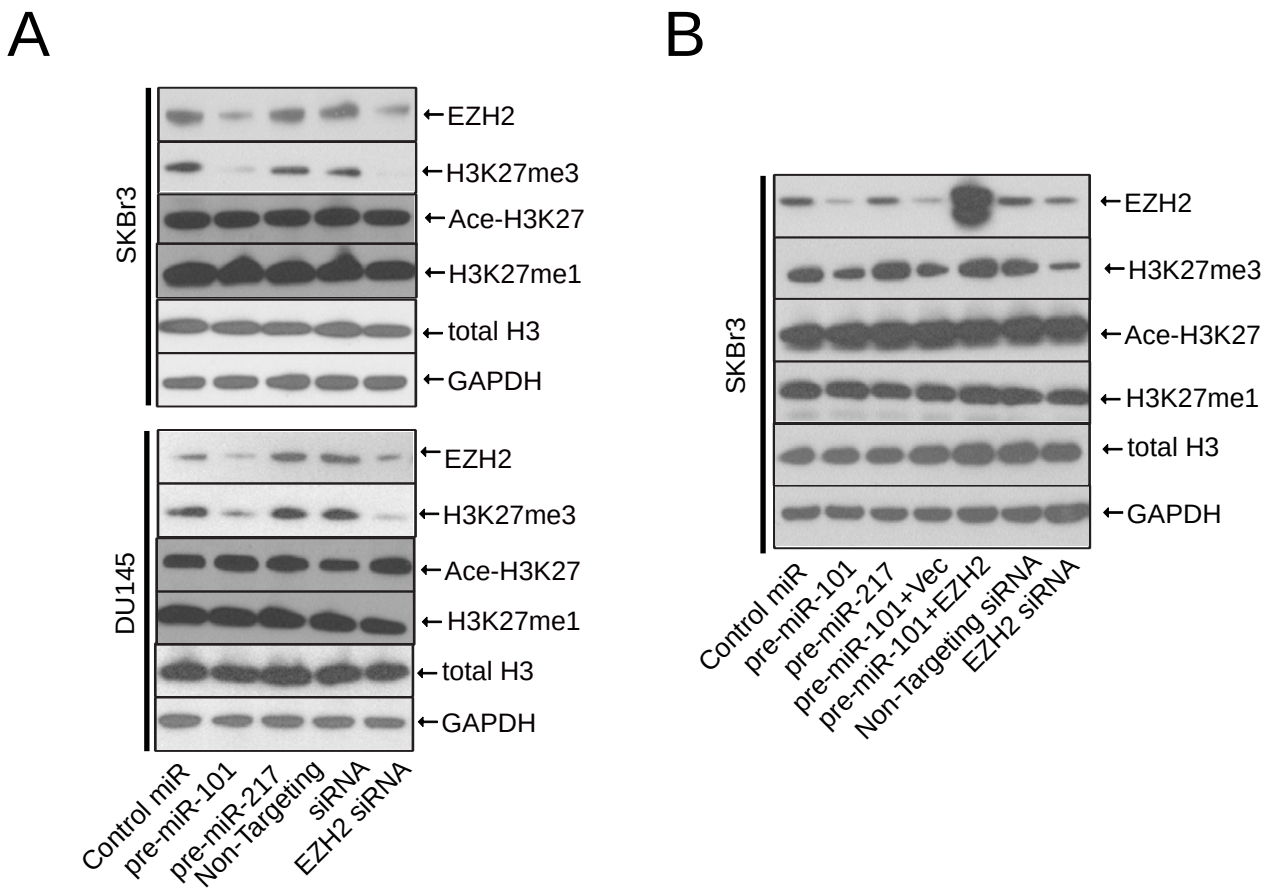

Figure S10. miR-101 expression reduces global histone H3 lysine 27 tri-methylation in cancer cell lines. (A) Immunoblot analysis was performed using cell lysates from SKBr3 and DU145 cells treated with miR-101, control miR as well as miR-217. EZH2 and tri-methyl H3-K27 antibodies were used to probe the blot. Blots were re-probed for total histone H3 as well as GAPDH levels. A representative blot of three independent experiments is shown. (**B**) miR-101 inhibition of H3K27 trimethylation is blocked by over-expression of ectopic EZH2 lacking an endogenous 3'UTR. Immunoblot analysis as in **A**, except SKBr3 cells were treated/transfected as indicated.

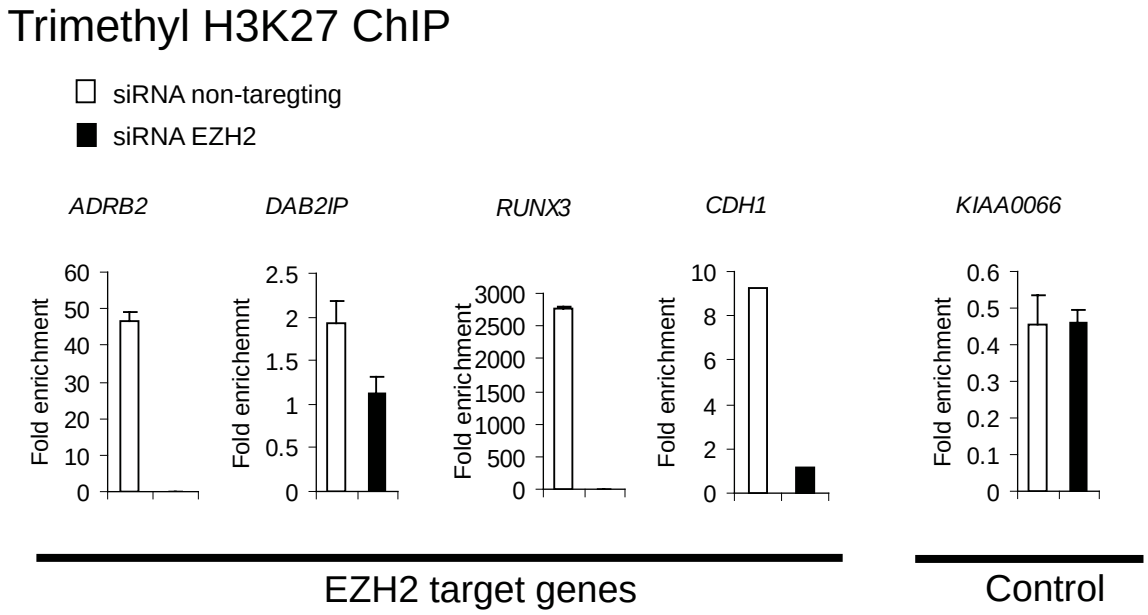

Figure S11. Chromatin immunoprecipitation (ChIP) assay of trimethyl H3K27 histone mark in SKBr3 cells transfected with EZH2 specific siRNA. Known EZH2 repression targets were examined. ChIP was performed to test H3K27 trimethylation at the promoters of ADRB2, DAB2IP, RUNX3 and CDH1 . KIAA0066 promoter served as control.

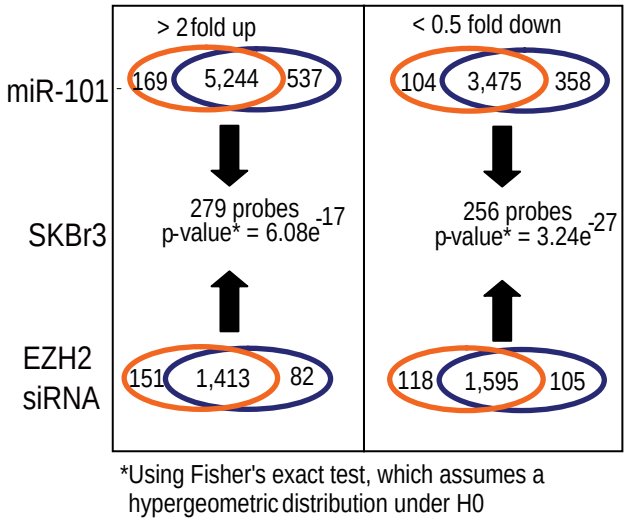

Figure S12. Gene expression array analysis of miR-101 overexpressing and EZH2 siRNA transfected SKBr3 cells. Fisher's exact test was performed on the gene expression profiles of SKBr3 cells overexpressing miR-101 and SKBr3 cells transfected with EZH2 siRNA. Analysis was performed on biological replicate samples (replicate 1 - orange circles; replicate 2 - blue circles). Overall, 279 and 256 probes were up- and down-regulated in both treatments, respectively, with p-values < 0.001.

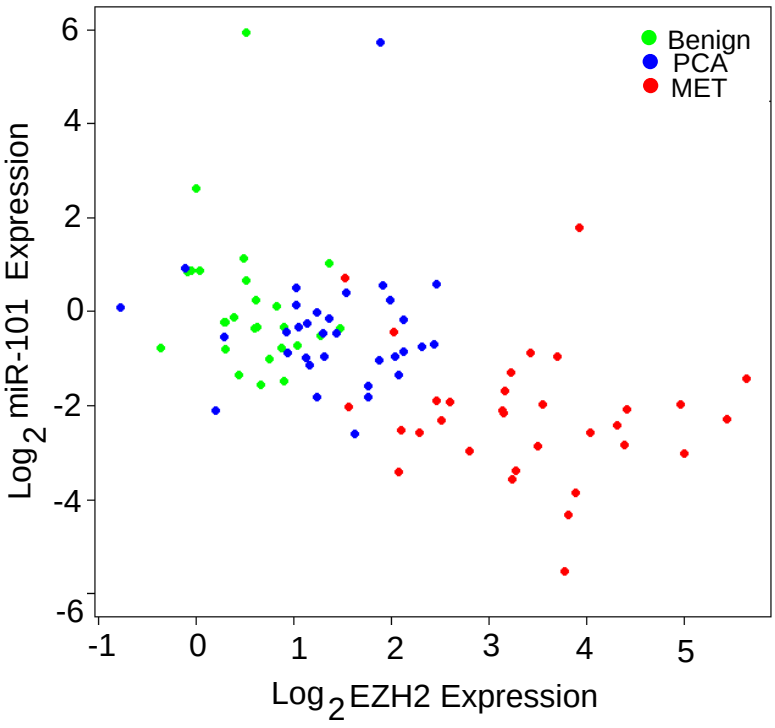

Figure S13. Inverse correlation between expression of miR-101 and EZH2 in prostate cancer progression. Horizontal axis depicts log2-transformed EZH2 expression relative to normal prostate RNA pool for N=91 prostate tissues (26 benign adjacent, 33 localized cancer, 32 metastatic). Vertical axis depicts $\log_2$-transformed miR-101 expression relative to U6 from the same set of samples. The correlation coefficient is -0.53 (95% CI: -0.66, -0.36, $p < 0.0001$). In contrast, EZH2 expression was not significantly correlated with miR-217 expression for this set of samples ($p = 0.21$).

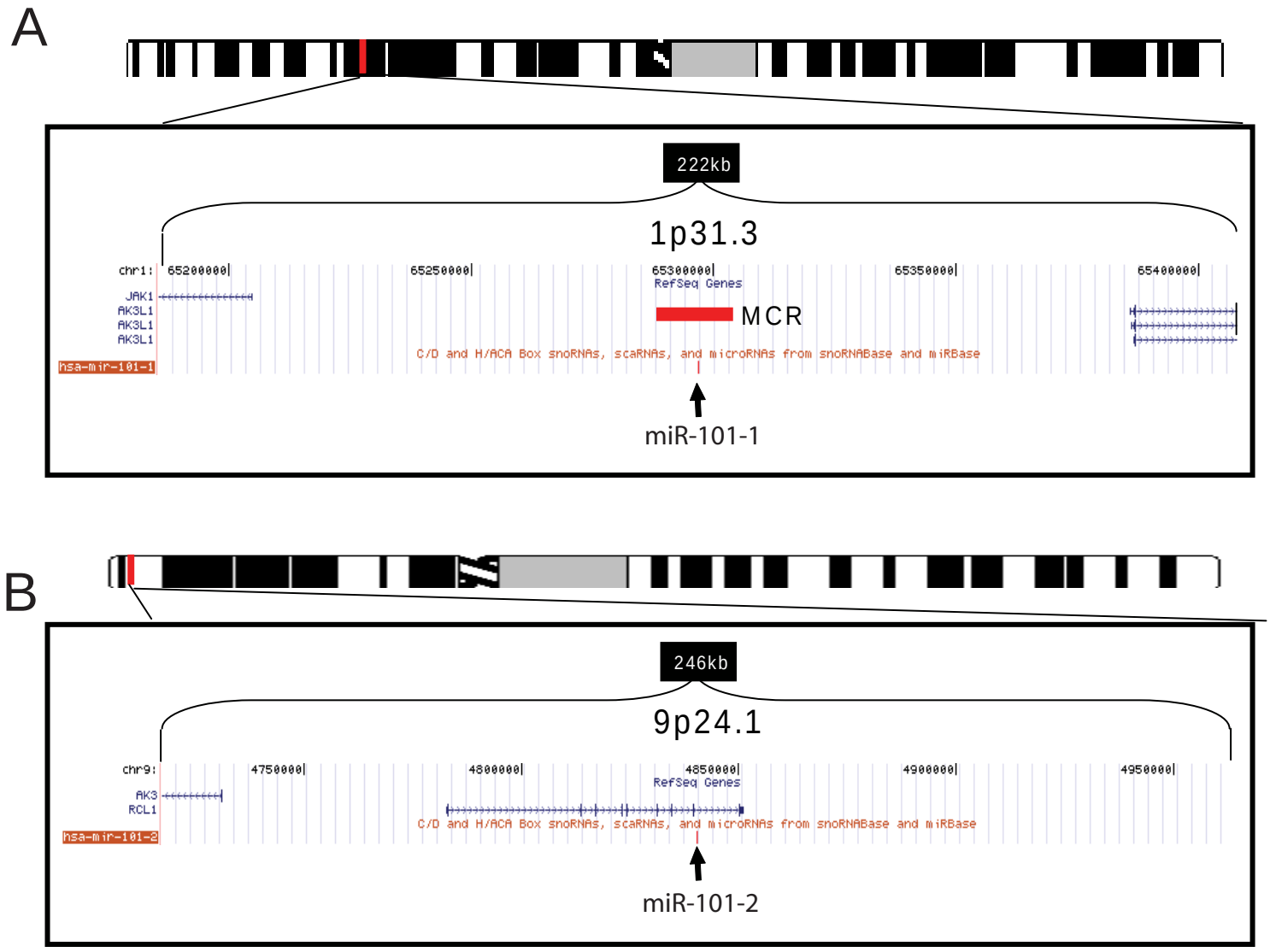

Figure S14. Genomic organization of miR-101-1 (A) and miR-101-2 (B) on chromosome 1p31.3 and 9p24, respectively. Horizontal red bar indicates the minimal common region of deletion (21kb) for miR-101-1 identified in breast and gastric cancers by high resolution array CGH. Area shown in braces indicate the absence of tumor suppressors located within about 100 kb flanking miR-101-1 and miR-101-2.

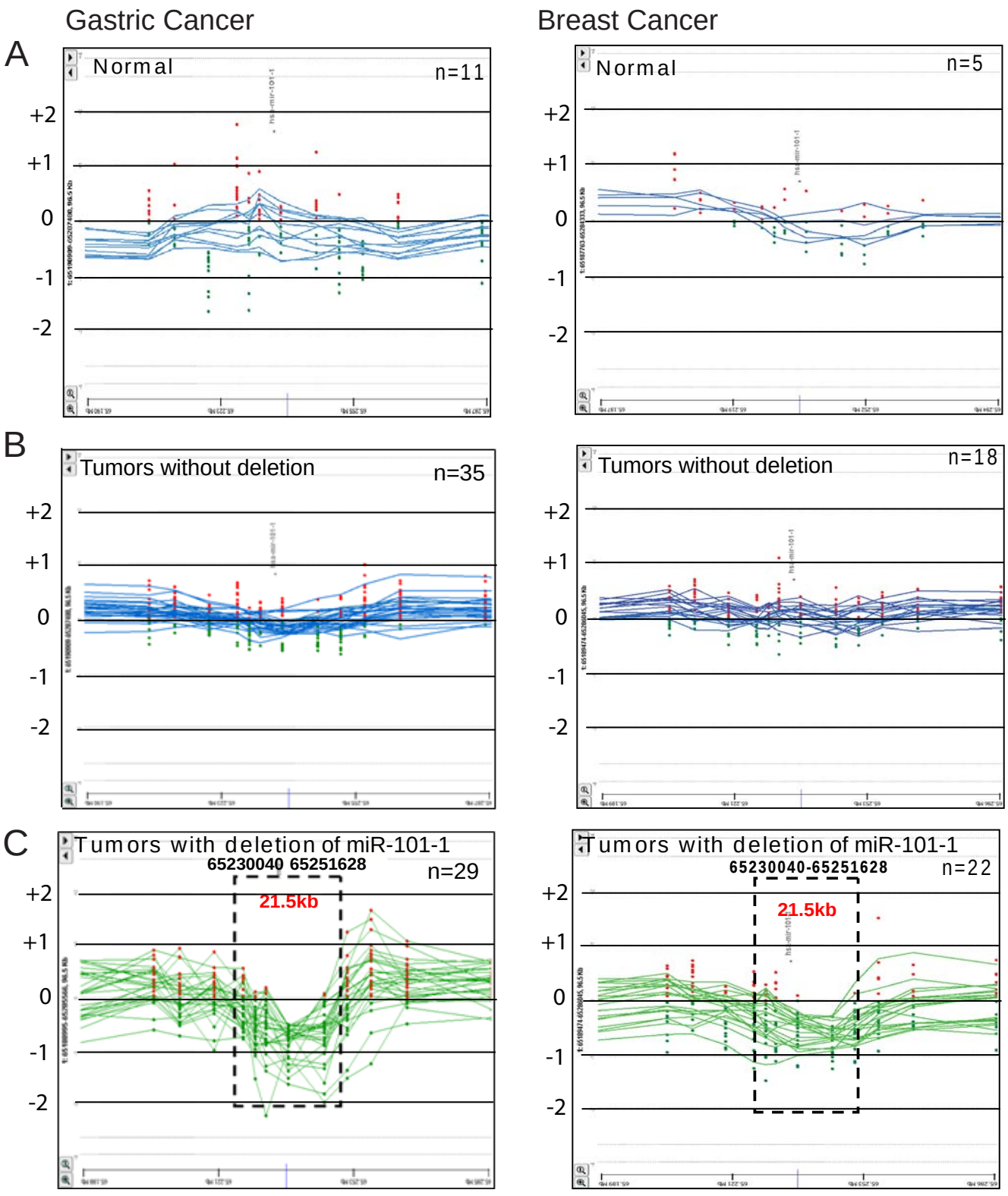

Figure S15. Focal genomic loss of the miR-101-1 locus in gastric and breast tumors. High resolution comparative genomic hybridization analysis of breast and gastric cancers show a focal deletion of about 21.5kb (area shown in dotted lines) containing miR-101-1 in a subset of tumors (**C**). A subset of tumors (**B**) and benign samples (**A**) did not show the focal deletion. Horizontal green and blue lines correspond to the ratio profile for copy number changes in each sample and the red and green dots indicate the probes represented on the array platform (Agilent 244K arrayCGH).

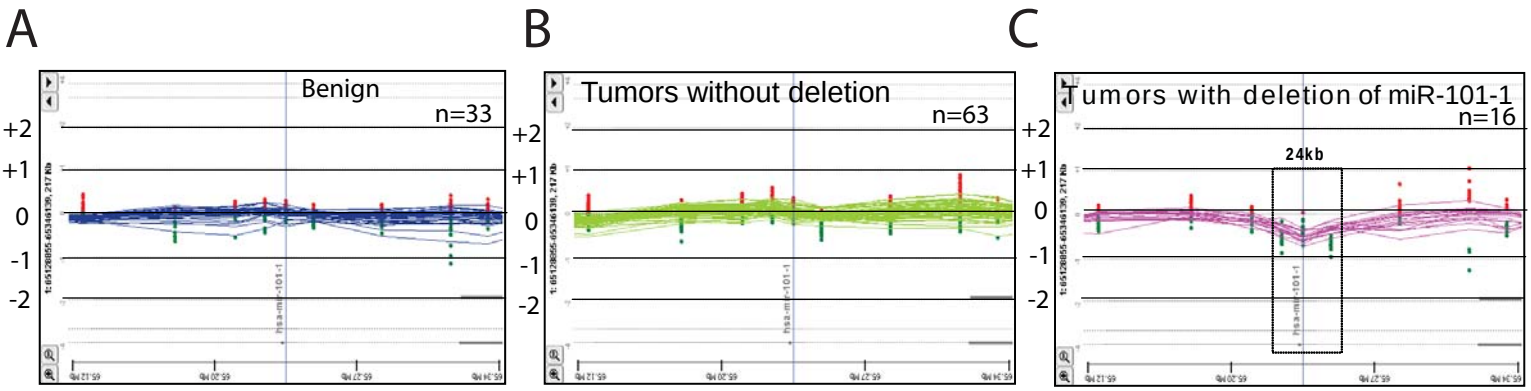

Figure S16. Focal genomic loss of the miR-101-1 locus in prostate cancer
Array comparative genomic hybridization analysis of benign adjacent normal (**A**) and tumors without miR-101 loss (**B**) and those with miR-101 loss (**C**). As in Fig. S15 except 105K array CGH was empolyed. The region of loss is approximately 24kb.

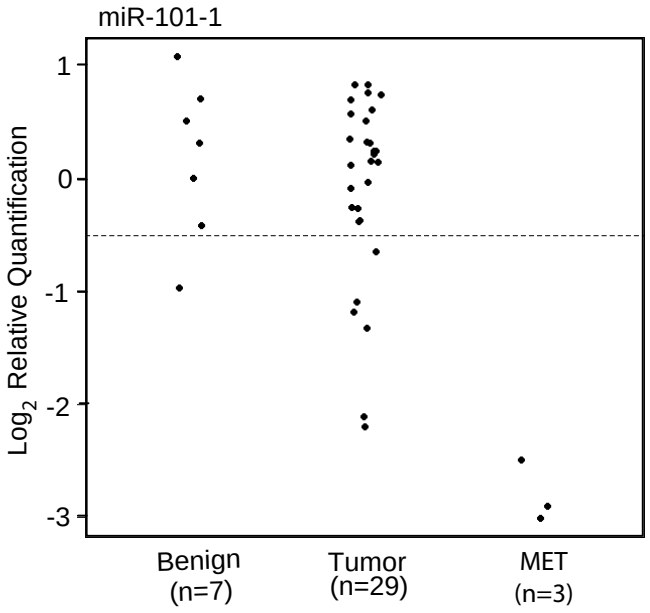

Figure S17. Genomic PCR of miR-101-1 in breast cancer. Vertical axes represent log(base 2) relative quantification values; dashed line is shown at the deletion threshold of $\log_2(0.7) \approx -0.51$. For clarity, points have been horizontally displaced within each sample class.

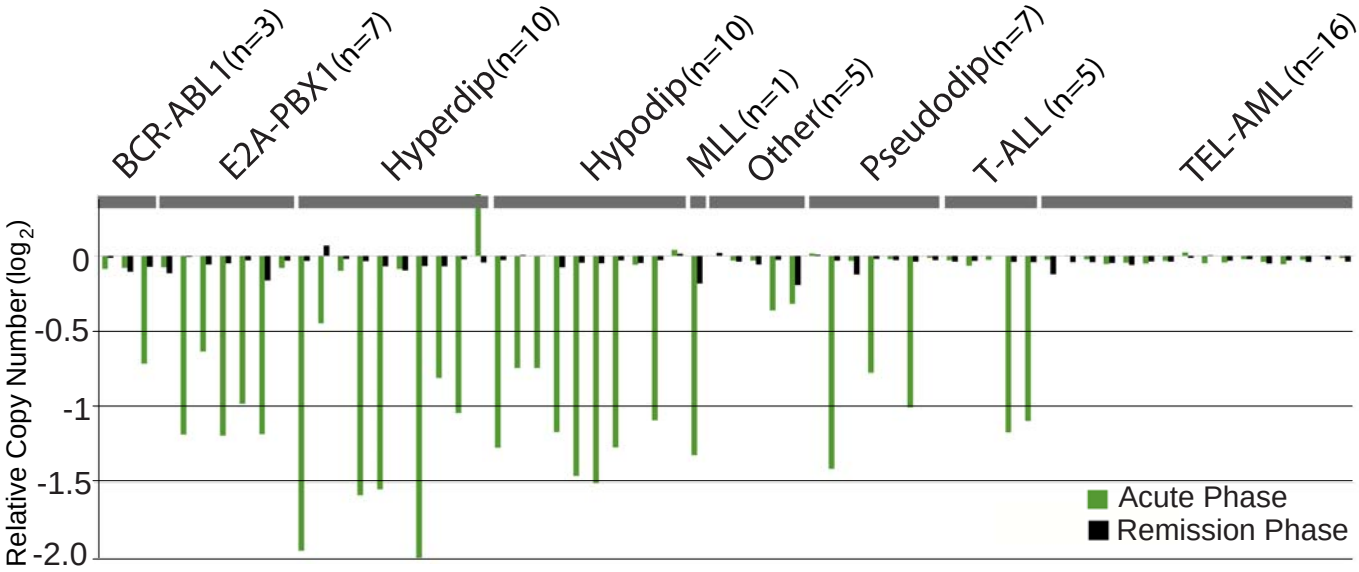

Figure S18. Comparison of the DNA copy number data in the acute phase and remission phase of acute lymphoblastic leukemia patients with miR-101-2 loss.
(Data from Mullighan CG et al, Nature 2007 Apr 12; 446(7137):758-64).

Supplementary Tables

Supplementary Table S1. Prediction of microRNAs that target EZH2. Ranking of binding sites that were predicted by three or more programs displayed relative to the score calculated by each respective program. The number in parenthesis represents miRNAs with multiple binding sites.

miRNA	MicroInspector	PicTar	TargetScan	miRanda
hsa-miR-101	1	1(2)	2(2)	1(2)
hsa-miR-151	2			
has-miR-124a		3(2)	6	8
hsa-miR-17-3p	3			
has-miR-126*		19		
has-miR-138		6(2)	4	5
has-miR-144		4(2)		
hsa-miR-181a	4			
hsa-miR-181b	5			
hsa-miR-185	6(2)	18		9
has-miR-199a*		5(2)		
has-miR-20a	7	18		
has-miR-20b		13		
hsa-miR-214	8			9
hsa-miR-217	9	2(2)	1(2)	3
hsa-miR-25	10		5	
has-miR-26a		17	3	
has-miR-26b		16	3	
has-miR-32		15	5	
hsa-miR-324-3p	11			
hsa-miR-330	12(2)			10
has-miR-363			5	
has-miR367			5	
has-miR-506			7	
has-let-7b		8	8	4
has-let-7i		9	8	6
has-let-7c		10	8	4
has-let-7g		10	8	6
has-let-7d		11	8	4
has-let-7e		12	8	6
has-let-7f		12	8	2
has-let-7a		12	8	4
has-miR-92		14	5	
has-miR-98		7	8	7

Supplementary Table S2. TargetScan predicted miR-101 binding sites for control genes, where applicable.

Gene	miR101 binding sites*			
SUZ12				
ARID1A	5' ...UGUAGACCCUUUCAU-GUACUGUA... ||| ||||||| 3' GAAGUCAAUAGUGUCAUGACAU	5' ...ACCCUUUCAUGUACUGUACUGUA... || ||||||| 3' GAAGUCAAUAGUGU-CAUGACAU	5' ...GUACUGUACACCUGAUACUGUAA... || ||||| 3' GAAGUCAAUAGUGUC-AUGACAU	5' ...CUGAUACUGUAAACA--UACUGUAA... || ||||| 3' GAAGUCAAUAGUGUCAUGACAU
FBN2	5' ...AAAGGCAACCGUGGUUACUGUAU... || ||||| 3' GAAGUCAAUAGUGUC--AUGACAU	5' ...AUUGCAGGCCAAACCGUACUGUA... ||| ||||||| 3' GAAGUCAAUAGUGUCAUGACAU		
C-FOS	5' ...AAUAGCUAUAUCCAUGUACUGUA... |||| ||||||| 3' GAAGUCAAUAGUGUCAUGACAU			
MYCN	5' ...GAAGUUCAUACCUAAGUACUGUA... |||| ||||||| 3' GAAGUCAAUAGUGU---CAUGACAU	5' ...GUUAAUCUCUGUUAU----GUACUGUA... ||||| ||||||| 3' GAAGUCAAUAGUGUCAUGACAU		
GAPDH				

***Predicted consequential pairing of target region (top) and miRNA (bottom)**

Supplementary Table S3. Meta-analysis of miR-101 expression in literature

Cancer Type	First Autho	Citation	Pubmed ID	Cancer(n)	Normal(n)	Expression	Percentile
Breast	Iorio	Cancer Research 2005; 65(16):7065-70	16461460	76	10	Down	5th
Lung	Yanaihara	Cancer Cell 2006; 9(3):189-98	16530703	104	104	Down	11th
Ovarian	Iorio	Cancer Research 2007; 67(18):8699-707	17875710	74	15	Down	7th
Thyroid	Visone	Oncogene 2007; 26(54):7590-5	17563749	10	10	-	-
Prostate	Porkka	Cancer Resarch 2007; 67(13):6130-5	17616669	9	4	-	-
Colon	Schepeler	Cancer Research 2008; 68(15):6416-24	18676867	49	10	Down	7th
All	Lu	Nature 2005; 435(7043):834-8	15944708	140	46	Down	2nd

Supplementary Table S4. QPCR Primers sequences used for monitoring transcript expression.

Gene name	Forward primer	Reverse primer
EZH2	TGCAGTTGCTTCAGTACCCATAAT	ATCCCCGTGTACTTTCCCATCATAAT
ADRB2	TTCCTCTTTGCATGGAATTTG	AGAGGAGTGGGGGAAGAGTC
hDAB2IP	TGGACGATGTGCTCTATGCC	GGATGGTGATGGTTTGGTAG
RUNX3	TCTGTAAGGCCCAAAGTGGGTA	ACCTCAGCATGACAATATGTCACAA
CIITA	CCGACACAGACACCATCAAC	CTTTTCTGCCCAACTTCTGC
CDH1	GGAGGAGAGCGGTGGTCAAA	TGTGCAGCTGGCTCAAGTCAA
GAPDH	TGCACCACCAACTGCTTAGC	GGCATGGACTGTGGTCATGAG

Supplementary Table S5. RQ estimation to determine threshold for single copy loss in male genomic DNA

Gene location	genomic region	RQ
chr1:65,296,708-65,296,562	miR101-1	1.14
chr2:56,063,616-56,063,502	miR217	1.37
chrX:45490429-45490738	miR221	0.46
chrX:45491265-45491574	miR222	0.56
chrX:133508210-133508507	miR424	0.56
chrX:113964173-113964483	miR448	0.63
chrX:133507924-133508194	miR503	0.67
chrX:137577438-137577720	miR504	0.56
chrX:118664629-118664939	miR766	0.66
chrX:77247072-77247271	PGK1	0.54
chrX:77247822-77248021	PGK2	0.48
chrX:77248872-77249071	PGK3	0.55
chr6: 170720579-170720690	TBP	1

Supplementary Table S6. Primer sequences used for genomic PCR assays

miR101-1	GTACTGTGATAACTGAAGGATG	ATTCTGCTTCTCTTTGCCTTGT
miR101-2	GACTGAACTGTCCTTTTTCGG	CCTTTCTCAATGTGATGGCA
miR217	CTAATGCATTGCCTTCAGCA	TTAGCATCTTGGGCTCACCT
miR424	ACCTGGTGGCAGGAACAC	TGAGGCGCTGCTATACCC
miR503	CAGGCGATGGCCTAAGACT	CAGGGTAAGTCTGGGACTGC
miR766	TGAAGACTCTGGGGACTTTTG	AATATACACAGAGGATTGCTTAGCC
miR448	TGGCTGGTTGCATATGTAGG	TGGTGTTTCTGGTGTCTGTCA
miR384	AAAACAAATGTTGCAATCCAAA	TGCAAATAACAAGATGCCTGA
miR222	ACTGAGCCATTGAGGGTACCTA	CCCCAGAAGGCAAAGGAT
miR221	GTGAGACAGCCAATGGAGAAC	TGTTCGTTAGGCAACAGCTACA
miR934	CAGCCTTTGATGGTGTGTGT	TCCATTACTGGAGACTCTGGG
TBP	TTAGCTGGCTCTGAGTATGAATAAC	GCTGGAAAACCCAACTTCTG

Supplementary Table S7. QPCR Primer sequences used for chromatin immunoprecipitation.

Gene name	Forward primer	Reverse primer
ADRB2	GTGACTTTATGCCCCTTTAGAGACAA	GAAGGGCTACAACTGGAACTGGAATA
DAB2IP	ATTCCTCCAGGTGGGTGTGG	CTAAGCCGCTGTTGCCTTGGC
CIITA	TCCTGGCCCGGGGCCTGG	CTGTTCCCCGGGCTCCCGC
RUNX3	TGTCCCGGGATCCTCTTCT	TAGAGACGTTGGTGCGGAAAT
CDH1	TAGAGGGTCACCGCGTCTAT	TCACAGGTGCTTTGCAGTTC
WNT1	GTTTCTGCTACGCTGCTGCT	CACCAGCTCACTTACCACCA
GAPDH	TACTAGCGGTTTTACGGGCG	TCGAACAGGAGGAGCAGAGAGCGA
KIAA0066	CTAGGAGGGTGGAGGTAGGG	GCCCCAAACAGGAGTAATGA
NUP214	CAGTGAGGTCTCAGCATCAGCA	CTGGAGGCTATGGGGGTACTTG

Supplementary Table S8. Array CGH data flanking the miR-101 and miR-217 genomic loci in prostate cancer

A	B	C	D	E	F
gene	hsa-mir-101-1	hsa-mir-101-1	hsa-mir-217	hsa-mir-101-2	hsa-mir-101-2
probe	A_16_P15150840	A_16_P15150873	A_16_P35687642	A_16_P02051568	A_16_P18537000
chromosome	chr1:065227167-224	chr1:065237759-818	chr2:056060746-805	chr9:004831297-356	chr9:004839536-595
CAP_M_1	-0.0809	-0.0809	-0.0341	-0.2261	-0.2261
CAP_M_10	-0.7481	-0.7481	0.216	-0.0775	-0.0775
CAP_M_11	0.0254	0.0254	0.0284	0.0112	0.0112
CAP_M_12	-0.2665	-0.2665	0.4022	0.2973	0.2973
CAP_M_13	-0.0141	-0.0141	0.2593	0.0282	0.0282
CAP_M_14	-1.8143	-1.8143	-0.1059	0.0951	0.0951
CAP_M_15	-1.227	-1.227	0.1283	-0.1659	-0.1659
CAP_M_16	0.1715	0.1715	0.2321	-0.5019	-0.5019
CAP_M_17	0.0705	0.0705	0.24	-0.8308	-0.8308
CAP_M_18	0.8552	0.8552	-1.3471	0.0101	0.0101
CAP_M_19	0.0659	0.0659	0.5654	0.4472	0.4472
CAP_M_2	-0.0776	-0.0776	-0.0611	-0.0883	-0.0883
CAP_M_20	-0.0085	-0.0085	-0.5042	0.7471	0.7471
CAP_M_21	0.1826	0.1826	-0.0842	-0.0834	-0.0834
CAP_M_22	0.1887	0.1887	0.2508	0.6486	0.6486
CAP_M_23	-0.4859	-0.4859	0.1719	-0.5443	-0.5443
CAP_M_24	0.0769	0.0769	0.2559	0.6235	0.6235
CAP_M_26	-0.0956	-0.0956	-0.1266	-0.1389	-0.1389
CAP_M_27	0.0822	0.0822	0.5059	0.0579	0.0579
CAP_M_28	-0.0821	-0.0821	-0.1024	0.3122	0.3122
CAP_M_29	-0.0525	-0.0525	-5.00E-04	-1.5964	-1.5964
CAP_M_3	0.0193	0.0193	-0.0267	0.3568	0.3568
CAP_M_30	-0.1362	-0.1362	0.0664	-0.2614	-0.2614
CAP_M_31	-0.1079	-0.1079	-0.1385	-0.102	-0.102
CAP_M_33	-0.0651	-0.0651	-0.0839	-0.1168	-0.1168
CAP_M_34	-1.0769	-1.0769	-0.0277	-0.0223	-0.0223
CAP_M_36	-0.0137	-0.0137	-0.5804	-0.5466	-0.5466
CAP_M_37	0.0191	0.0191	0.0183	0.0017	0.0017
CAP_M_38	-0.0443	-0.0443	-0.0407	0.5421	0.5421
CAP_M_39	-0.2888	-0.2888	-0.0374	0.7081	0.7081
CAP_M_4	-0.0164	-0.0164	-0.046	-0.3367	-0.3367
CAP_M_40	-0.4486	-0.4486	0.1381	-0.1165	-0.1165
CAP_M_41	-0.7118	-0.7118	-0.0902	-0.1655	-0.1655
CAP_M_43	-0.0754	-0.0754	0.1981	-0.1125	-0.1125
CAP_M_44	-0.0795	-0.0795	-0.0492	-0.0952	-0.0952
CAP_M_5	0.2263	0.2263	-0.3897	-0.1157	-0.1157
CAP_M_6	-0.0604	-0.0604	-0.06	-0.6029	-0.6029
CAP_M_7	-0.3393	-0.3393	-0.2452	0.059	0.059
CAP_M_8	-1.2465	-1.2465	-0.0276	-0.039	-0.039
CAP_M_9	0.1546	0.1546	0.0894	0.1187	0.1187
CAP_N_1	0.0292	0.0292	-0.0197	-0.0081	-0.0081
CAP_N_10	0.0077	0.0077	-0.0087	-0.0043	-0.0043
CAP_N_11	-0.0026	-0.0026	-0.003	-0.0113	-0.0113
CAP_N_12	-0.0024	-0.0024	-0.0044	-0.0054	-0.0054
CAP_N_13	0.0445	0.0445	0.2069	-0.1313	-0.1313
CAP_N_14	0.0386	0.0386	0.0932	-0.0876	-0.0876
CAP_N_15	0.0217	0.0217	0.0673	-0.0161	-0.0161
CAP_N_16	-0.0439	-0.0439	-0.0163	-0.0246	-0.0246
CAP_N_17	0.0071	0.0071	-0.0039	-0.0041	-0.0041
CAP_N_18	-0.3788	-0.3788	0.2451	0.0546	0.0546
CAP_N_19	0.0662	0.0662	0.008	0.0469	0.0469
CAP_N_2	-0.0021	-0.0021	-0.0104	-0.0143	-0.0143
CAP_N_20	-0.074	-0.074	-0.029	-0.0432	-0.0432
CAP_N_21	-0.0157	-0.0157	0.009	-0.0115	-0.0115
CAP_N_22	0.0105	0.0105	0.011	-0.009	-0.009
CAP_N_23	-0.0251	-0.0251	0.0037	0.0022	0.0022
CAP_N_24	-0.0093	-0.0093	0.005	0.0164	0.0164
CAP_N_25	0.0548	0.0548	0.0156	0.0377	0.0377
CAP_N_26	6.00E-04	6.00E-04	0.0016	0.014	0.014
CAP_N_27	-0.0247	-0.0247	-0.0086	-0.0198	-0.0198
CAP_N_28	-0.0164	-0.0164	-0.0413	-0.0168	-0.0168
CAP_N_29	-0.0306	-0.0306	-0.0222	-0.0373	-0.0373
CAP_N_3	-0.0385	-0.0385	-0.0157	-0.037	-0.037
CAP_N_30	-0.0157	-0.0157	-0.0163	-0.0174	-0.0174
CAP_N_31	-0.0322	-0.0322	-0.0458	-0.0559	-0.0559
CAP_N_32	-0.0379	-0.0379	-0.0409	-0.037	-0.037
CAP_N_33	-0.0449	-0.0449	-0.0446	-0.0344	-0.0344
CAP_N_4	-0.0529	-0.0529	-0.0172	-0.0183	-0.0183

CAP_N_5	-0.0572	-0.0572	-0.0188	-0.0814	-0.0814
CAP_N_6	-0.2773	-0.2773	0.2397	-0.0202	-0.0202
CAP_N_7	-0.2018	-0.2018	0.2087	-0.0106	-0.0106
CAP_N_8	0.0197	0.0197	-0.0084	-0.0168	-0.0168
CAP_N_9	-0.0368	-0.0368	-0.0048	-0.0385	-0.0385
CAP_T_1	-0.033	-0.033	-0.0268	-0.0179	-0.0179
CAP_T_10	0.0026	0.0026	0.0079	0.0078	0.0078
CAP_T_11	-0.0648	-0.0648	-0.0331	-0.0468	-0.0468
CAP_T_12	-0.0225	-0.0225	-0.0225	-0.0313	-0.0313
CAP_T_17	0.0303	0.0303	-0.0172	-0.0928	-0.0928
CAP_T_18	-0.0031	-0.0031	0.0401	0.124	0.124
CAP_T_19	-0.0254	-0.0254	-0.0078	-0.0311	-0.0311
CAP_T_2	-0.0243	-0.0243	-0.0203	-0.0257	-0.0257
CAP_T_20	-0.03	-0.03	-0.0197	-0.0191	-0.0191
CAP_T_21	-0.0237	-0.0237	-0.0068	-0.0206	-0.0206
CAP_T_22	-0.0154	-0.0154	-0.0027	-0.0065	-0.0065
CAP_T_23	-0.065	-0.065	-0.0311	-0.1297	-0.1297
CAP_T_24	0.0493	0.0493	-0.0278	-2.00E-04	-2.00E-04
CAP_T_25	-0.0399	-0.0399	-0.0246	0.0098	0.0098
CAP_T_26	0.0332	0.0332	0.0084	0.0112	0.0112
CAP_T_27	0.043	0.043	0.0587	0.0578	0.0578
CAP_T_28	0.0093	0.0093	0.0062	-0.0095	-0.0095
CAP_T_29	0.0272	0.0272	0.0077	0.0064	0.0064
CAP_T_3	-0.0036	-0.0036	-0.0032	-0.0148	-0.0148
CAP_T_30	0.0052	0.0052	-0.0071	-0.012	-0.012
CAP_T_31	0.043	0.043	0.0118	0.0095	0.0095
CAP_T_32	0.0327	0.0327	0.0104	-0.0558	-0.0558
CAP_T_33	0.0821	0.0821	0.085	0.0837	0.0837
CAP_T_34	0.0432	0.0432	0.0734	0.0637	0.0637
CAP_T_35	0.0947	0.0947	0.0686	0.0798	0.0798
CAP_T_36	-0.0273	-0.0273	-0.0307	-0.1164	-0.1164
CAP_T_37	-0.3564	-0.3564	-0.0041	-0.0059	-0.0059
CAP_T_38	0.0696	0.0696	0.0516	0.0602	0.0602
CAP_T_39	0.024	0.024	0.0072	0.0046	0.0046
CAP_T_4	-0.0269	-0.0269	-0.0237	-0.0314	-0.0314
CAP_T_40	-0.0011	-0.0011	0.0031	-0.0656	-0.0656
CAP_T_41	-0.0571	-0.0571	-0.0246	-0.0198	-0.0198
CAP_T_42	-0.0357	-0.0357	-0.0141	-0.0233	-0.0233
CAP_T_43	-0.0245	-0.0245	-0.005	-0.0039	-0.0039
CAP_T_44	0.0221	0.0221	0.0186	-0.0054	-0.0054
CAP_T_45	0.0246	0.0246	0.0323	-0.0205	-0.0205
CAP_T_46	-0.0117	-0.0117	0.0055	-0.0064	-0.0064
CAP_T_47	-5.00E-04	-5.00E-04	-0.0317	-9.00E-04	-9.00E-04
CAP_T_48	0.0078	0.0078	0.0149	-0.0082	-0.0082
CAP_T_49	-0.0261	-0.0261	-0.0171	-0.0402	-0.0402
CAP_T_5	0.0324	0.0324	0.0265	0.0197	0.0197
CAP_T_50	-0.0291	-0.0291	-0.0303	-0.0232	-0.0232
CAP_T_51	-0.0171	-0.0171	-0.0117	-0.0127	-0.0127
CAP_T_52	-0.0076	-0.0076	3.00E-04	-0.0031	-0.0031
CAP_T_53	0.0279	0.0279	0.0194	0.0282	0.0282
CAP_T_54	0.0233	0.0233	0.0155	0.0089	0.0089
CAP_T_55	-0.0106	-0.0106	-0.0095	0.0134	0.0134
CAP_T_56	0.0013	0.0013	-3.00E-04	-0.0172	-0.0172
CAP_T_57	-0.0011	-0.0011	0.2039	-0.059	-0.059
CAP_T_58	-0.0473	-0.0473	0.0078	-0.0136	-0.0136
CAP_T_59	-0.0389	-0.0389	-0.0231	0.008	0.008
CAP_T_6	0.0313	0.0313	0.0385	0.0315	0.0315
CAP_T_60	0.0057	0.0057	0.003	-0.0219	-0.0219
CAP_T_61	0.0517	0.0517	-0.0359	0.0537	0.0537
CAP_T_62	0.0186	0.0186	0.0246	-0.5106	-0.5106
CAP_T_63	3.00E-04	3.00E-04	-0.0018	-0.0181	-0.0181
CAP_T_64	-0.0027	-0.0027	-0.0068	-0.0044	-0.0044
CAP_T_65	0.0126	0.0126	0.003	-0.6371	-0.6371
CAP_T_66	0.0518	0.0518	0.0555	0.0558	0.0558
CAP_T_67	-0.0566	-0.0566	-0.0458	-0.0568	-0.0568
CAP_T_68	-0.0214	-0.0214	-0.0096	-0.024	-0.024
CAP_T_69	0.0399	0.0399	-0.0339	-0.1082	-0.1082
CAP_T_7	-0.0214	-0.0214	0.0039	-0.0064	-0.0064
CAP_T_70	0.0295	0.0295	-0.0496	-0.0018	-0.0018
CAP_T_71	0.0606	0.0606	0.0522	0.0534	0.0534
CAP_T_72	0.0022	0.0022	-0.0073	-0.025	-0.025
CAP_T_73	0.0592	0.0592	0.1251	-0.0182	-0.0182
CAP_T_74	0.0034	0.0034	-0.0388	-0.0586	-0.0586

CAP_T_8	0.0381	0.0381	0.2094	-0.0287	-0.0287
CAP_T_9	-0.0012	-0.0012	0.0096	0.0053	0.0053

*Column B to F represents log 2 transformed Relative probe intensity compared to normal

Supplementary Table S9. Array CGH data flanking the miR-101 and miR-217 genomic loci in breast cancer

A	B	C	D	E	F	G	H	I	J	K	L
gene	hsa-mir-101-1	hsa-mir-217	hsa-mir-217	hsa-mir-217	hsa-mir-217	hsa-mir-217	hsa-mir-101-2	hsa-mir-101-2	hsa-mir-101-2	hsa-mir-101-2	hsa-mir-101-2
probe	A_16_P15150753	A_16_P15663086	A_16_P15663091	A_16_P00379781	A_16_P00379785	A_16_P35687829	A_16_P02051568	A_16_P02051579	A_16_P18537000	A_16_P18537015	A_16_P02051603
chromosome	chr1:065242851-910	chr2:056057320-379	chr2:056063298-357	chr2:056066708-767	chr2:056069467-526	chr2:056072286-345	chr9:004831297-356	chr9:004835518-577	chr9:004839536-595	chr9:004843002-061	chr9:004846324-383
BRE_T_251469311676	-0.1405	-0.0526	-0.0526	-0.0526	-0.0526	-0.0526	-0.0249	-0.0249	-0.0249	-0.0249	-0.0249
BRE_T_251469311684	0.0633	0.0552	0.0552	0.0552	0.0552	0.0552	0.0277	0.0277	0.0277	0.0277	0.0277
BRE_T_251469312771	-0.1507	0.1227	0.1227	-0.1606	-0.1606	-0.1606	-0.2997	-0.2997	-0.2997	-0.2997	-0.2997
BRE_T_251469313214	-0.6194	-0.1427	-0.1427	-0.1427	-0.1427	-0.1427	0.0304	0.0304	0.0304	0.0304	0.0304
BRE_T_251469313216	-0.1489	-0.1194	-0.1194	-0.1194	-0.1194	-0.1194	-0.1838	-0.1838	-0.1838	-0.1838	-0.1838
BRE_T_251469313218	-0.3294	-0.1703	-0.1703	-0.1703	-0.1703	-0.1703	-0.1704	-0.1704	-0.1704	-0.1704	-0.1704
BRE_T_251469313119	-0.2423	-0.2342	-0.2342	-0.2342	-0.2342	-0.2342	-0.1426	-0.1426	-0.1426	-0.1426	-0.1426
BRE_T_251469313120	-0.181	-0.292	-0.292	-0.292	-0.292	-0.292	-0.0842	-0.0842	-0.0842	-0.0842	-0.0842
BRE_T_251469313121	-0.4907	-0.2527	-0.2527	-0.2527	-0.2527	-0.2527	-0.3054	-0.3054	-0.3054	-0.3054	-0.3054
BRE_T_251469313127	0.0177	0.0968	0.0968	0.0968	0.0968	0.0968	-0.2564	-0.2564	-0.2564	-0.2564	-0.2564
BRE_T_251469313123	-0.0355	-0.0524	-0.0524	-0.0524	-0.0524	-0.0524	0.0224	0.0224	0.0224	0.0224	0.0224
BRE_T_251469313124	-0.3114	-0.1618	-0.1618	-0.4111	-0.4111	-0.4111	-0.0285	-0.0285	-0.0285	-0.0285	-0.0285
BRE_T_251469313126	-0.1129	0.0504	0.0504	0.0504	0.0504	0.0504	0.777	0.777	0.777	0.777	0.777
BRE_T_251469315119	-0.2651	0.0247	0.0247	-0.2031	-0.2031	-0.2031	-0.2296	-0.2296	-0.2296	-0.2296	-0.2296
BRE_N_251469320976	-0.2035	-0.0194	-0.0194	-0.0194	-0.0194	-0.0194	-0.1976	-0.1976	-0.1976	-0.1976	-0.1976
BRE_T_251469313217	-0.2606	-0.0769	-0.0769	-0.0769	-0.0769	-0.0769	-0.0879	-0.0879	-0.0879	-0.0879	-0.0879
BRE_C_T47D_251469313393	-0.308	-0.2019	-0.2019	-0.2019	-0.2019	-0.2019	-0.306	-0.306	-0.306	-0.306	-0.306
BRE_C_MB231_251469311532	0.0144	-0.125	-0.125	-0.125	-0.125	-0.125	-0.9174	-0.9174	-0.9174	-0.9174	-0.9174
BRE_C_BT474_251469311572	-0.0021	-0.3202	-0.3202	-0.3202	-0.3202	-0.3202	-0.5394	-0.5394	-0.5394	-0.5394	-0.5394
BRE_C_SKBR3_251469311573	-0.0106	-0.1699	-0.1699	-0.1699	-0.1699	-0.1699	-0.0681	-0.0681	-0.0681	-0.0681	-0.0681
BRE_C_BT549_251469311675	-0.0665	-0.2431	-0.2431	-0.2431	-0.2431	-0.2431	0.1949	0.1949	0.1949	0.1949	0.1949
BRE_C_CAMA_251469313394	-0.6408	-0.2301	-0.2301	-0.2301	-0.2301	-0.2301	0.2798	0.2798	0.2798	0.2798	0.2798
BRE_C_MCF7_251469311690	-0.3	0.1156	0.1156	0.1156	0.1156	0.1156	-0.1701	-0.1701	-0.1701	-0.1701	-0.1701
BRE_C_ZR75-1_251469311574	-0.4333	-0.0824	-0.0824	-0.0824	-0.0824	-0.0824	-0.0403	-0.0403	-0.0403	-0.0403	-0.0403
BRE_C_MB361_251469312813	-0.2184	-0.0537	-0.0537	-0.0537	-0.0537	-0.0537	-0.6366	-0.6366	-0.6366	-0.6366	-0.6366
BRE_T_251469320973	-0.1431	8.00E-04	8.00E-04	8.00E-04	8.00E-04	8.00E-04	-0.164	-0.164	-0.164	-0.164	-0.164
BRE_T_251469320974	0.0234	-0.4172	-0.4172	-0.4172	-0.4172	-0.4172	-0.1796	-0.1796	-0.1796	-0.1796	-0.1796
BRE_T_251469320975	0.0231	-0.1123	-0.1123	-0.1123	-0.1123	-0.1123	-0.5827	-0.5827	-0.5827	-0.5827	-0.5827
BRE_T_251469313196	0.0595	-0.1514	-0.1514	-0.1514	-0.1514	-0.1514	-0.0493	-0.0493	-0.0493	-0.0493	-0.0493
BRE_T_251469313197	-0.0024	-0.2514	-0.2514	-0.2514	-0.2514	-0.2514	0.0638	0.0638	0.0638	0.0638	0.0638
BRE_T_251469313128	-0.0353	-0.2405	-0.2405	-0.2405	-0.2405	-0.2405	0.0396	0.0396	0.0396	0.0396	0.0396
BRE_T_251469313095	-0.1258	-0.3343	-0.3343	-0.3343	-0.3343	-0.3343	-0.1493	-0.1493	-0.1493	-0.1493	-0.1493
BRE_T_251469315118	0.0804	-0.1422	-0.1422	-0.1422	-0.1422	-0.1422	-0.6062	-0.6062	-0.6062	-0.6062	-0.6062
BRE_T_251469320968	0.1106	0.152	0.152	0.152	0.152	0.152	0.0938	0.0938	0.0938	0.0938	0.0938
BRE_N_251469315120	-0.0026	-0.0779	-0.0779	-0.0779	-0.0779	-0.0779	-0.0446	-0.0446	-0.0446	-0.0446	-0.0446
BRE_N_251469312770	0.205	-0.0217	-0.0217	-0.0217	-0.0217	-0.0217	0.3774	0.3774	0.3774	0.3774	0.3774
BRE_N_251469315122	0.0586	0.0246	0.0246	0.0246	0.0246	0.0246	0.0302	0.0302	0.0302	0.0302	0.0302
BRE_N_251469311688	0.0461	-0.021	-0.021	-0.021	-0.021	-0.021	0.0961	0.0961	0.0961	0.0961	0.0961
BRE_N_251469311677	0.2193	-0.0351	-0.0351	-0.0351	-0.0351	-0.0351	0.0052	0.0052	0.0052	0.0052	0.0052
BRE_C_BT483_251469311674	-0.0229	-0.2658	-0.2658	-0.2658	-0.2658	-0.2658	-0.3159	-0.3159	-0.3159	-0.3159	-0.3159
RE_C_MDAMB468_25146931157	0.2485	0.0897	0.0897	0.0897	0.0897	0.0897	-0.2353	-0.2353	-0.2353	-0.2353	-0.2353
BRE_C_MB436_251469312721	0.2064	0.0928	0.0928	0.0928	0.0928	0.0928	0.5755	0.5755	0.5755	0.5755	0.5755
BRE_N_MCF10A_251469311685	0.0281	-0.1803	-0.1803	-0.1803	-0.1803	-0.1803	-0.0984	-0.0984	-0.0984	-0.0984	-0.0984

*Column B to L represents log 2 transformed Relative probe intensity compared to normal

Supplementary Table S10. Array CGH data flanking the miR-101 and miR-217 genomic loci in gastric cancer

A	B	C	D	E	F	G	H	I	J	K	L
gene	hsa-mir-101-1	hsa-mir-217	hsa-mir-217	hsa-mir-217	hsa-mir-217	hsa-mir-217	hsa-mir-101-2	hsa-mir-101-2	hsa-mir-101-2	hsa-mir-101-2	hsa-mir-101-2
probe	A_16_P15150753	A_16_P15663086	A_16_P15663091	A_16_P00379781	A_16_P00379785	A_16_P35687829	A_16_P02051568	A_16_P02051579	A_16_P18537000	A_16_P18537015	A_16_P02051603
chromosome	chr1:065242851-910	chr2:056057320-379	chr2:056063298-357	chr2:056066708-767	chr2:056069467-526	chr2:056072286-345	chr9:004831297-356	chr9:004835518-577	chr9:004839536-595	chr9:004843002-061	chr9:004846324-383
STO_T_251469326325	0.044	-0.2346	-0.2346	-0.2346	-0.2346	-0.2346	0.0294	0.0294	0.0294	0.0294	0.0294
STO_T_251469326313	-0.101	-0.2465	-0.2465	-0.2465	-0.2465	-0.2465	-0.0865	-0.0865	-0.0865	-0.0865	-0.0865
STO_T_251469326322	-0.077	0.051	0.051	0.051	0.051	0.051	-0.1757	-0.1757	-0.1757	-0.1757	-0.1757
STO_T_251469326308	-0.0549	-0.077	-0.077	-0.077	-0.077	-0.077	0.0146	0.0146	0.0146	0.0146	0.0146
STO_T_251469326309	-0.1464	0.0683	0.0683	0.0683	0.0683	0.0683	-0.0551	-0.0551	-0.0551	-0.0551	-0.0551
STO_T_251469326323	-0.1651	-0.2547	-0.2547	-0.2547	-0.2547	-0.2547	0.1343	0.1343	0.1343	0.1343	0.1343
STO_T_251469324925	-0.024	-0.0885	-0.0885	-0.0885	-0.0885	-0.0885	0.1145	0.1145	0.1145	0.1145	0.1145
STO_T_251469324329	0.0735	-0.0766	-0.0766	-0.0766	-0.0766	-0.0766	-0.0436	-0.0436	-0.0436	-0.0436	-0.0436
STO_T_251469326314	-0.0585	0.075	0.075	0.075	0.075	0.075	-0.1587	-0.1587	-0.1587	-0.1587	-0.1587
STO_T_251469326324	-0.0233	0.0304	0.0304	0.0304	0.0304	0.0304	0.038	0.038	0.038	0.038	0.038
STO_T_251469324926	0.0641	0.0389	0.0389	0.0389	0.0389	0.0389	-0.0579	-0.0579	-0.0579	-0.0579	-0.0579
STO_T_251469324924	-0.0148	-0.0344	-0.0344	-0.0344	-0.0344	-0.0344	0.0457	0.0457	0.0457	0.0457	0.0457
STO_T_251469324945	-0.1118	-0.095	-0.095	-0.095	-0.095	-0.095	-0.1474	-0.1474	-0.1474	-0.1474	-0.1474
STO_T_251469324940	0.0066	0.0255	0.0255	0.0255	0.0255	0.0255	0.0331	0.0331	0.0331	0.0331	0.0331
STO_T_251469324943	-0.0601	0.1552	0.1552	0.1552	0.1552	0.1552	0.0316	0.0316	0.0316	0.0316	0.0316
STO_T_251469324944	-0.0754	-0.0959	-0.0959	-0.0959	-0.0959	-0.0959	-0.0327	-0.0327	-0.0327	-0.0327	-0.0327
STO_T_251469326260	0.1496	0.0621	0.0621	0.0621	0.0621	0.0621	-0.4201	-0.4201	-0.4201	-0.4201	-0.4201
STO_T_251469326259	-0.096	-0.2532	-0.2532	-0.2532	-0.2532	-0.2532	0.0178	0.0178	0.0178	0.0178	0.0178
STO_T_251469324408	-0.1419	0.1298	0.1298	0.1298	0.1298	0.1298	-0.1263	-0.1263	-0.1263	-0.1263	-0.1263
STO_T_251469324411	-0.0181	-0.0066	-0.0066	-0.0066	-0.0066	-0.0066	-0.1341	-0.1341	-0.1341	-0.1341	-0.1341
STO_T_251469324942	-0.1786	0.2448	0.2448	0.2448	0.2448	0.2448	-0.4843	-0.4843	-0.4843	-0.4843	-0.4843
STO_T_251469326258	-0.0628	-0.152	-0.152	-0.152	-0.152	-0.152	-0.0224	-0.0224	-0.0224	-0.0224	-0.0224
STO_T_251469324407	0.1514	-0.25	-0.25	-0.25	-0.25	-0.25	0.0358	0.0358	0.0358	0.0358	0.0358
STO_T_251469324410	-0.0868	-0.2653	-0.2653	-0.2653	-0.2653	-0.2653	-0.0949	-0.0949	-0.0949	-0.0949	-0.0949
STO_T_251469324759	-0.033	-0.0332	-0.0332	-0.0332	-0.0332	-0.0332	-0.1035	-0.1035	-0.1035	-0.1035	-0.1035
STO_T_251469326205	-0.1819	0.1354	0.1354	0.1354	0.1354	0.1354	-0.6817	-0.6817	-0.6817	-0.6817	-0.6817
STO_T_251469326207	-0.0839	-0.0855	-0.0855	-0.0855	-0.0855	-0.0855	0.0779	0.0779	0.0779	0.0779	0.0779
STO_T_251469326206	0.0388	-0.0468	-0.0468	-0.0468	-0.0468	-0.0468	-0.148	-0.148	-0.148	-0.148	-0.148
STO_T_251469326203	-0.0411	0.0291	0.0291	0.0291	0.0291	0.0291	-0.161	-0.161	-0.161	-0.161	-0.161
STO_T_251469324760	-0.1748	0.0928	0.0928	0.0928	0.0928	0.0928	0.2775	0.2775	0.2775	0.2775	0.2775
STO_T_251469326261	0.043	-0.1485	-0.1485	-0.1485	-0.1485	-0.1485	0.6387	0.6387	0.6387	0.6387	0.6387
STO_T_251469324761	0.0066	-0.0755	-0.0755	-0.0755	-0.0755	-0.0755	-0.3046	-0.3046	-0.3046	-0.3046	-0.3046
STO_T_251469326262	-0.0463	-0.169	-0.169	-0.169	-0.169	-0.169	-0.0196	-0.0196	-0.0196	-0.0196	-0.0196
STO_X_251469324762	-0.115	-0.0177	-0.0177	-0.0177	-0.0177	-0.0177	0.1415	0.1415	0.1415	0.1415	0.1415
STO_T_251469324757	-0.0477	0.0032	0.0032	0.0032	0.0032	0.0032	0.0073	0.0073	0.0073	0.0073	0.0073
STO_T_251469326204	0.1213	-0.1615	-0.1615	-0.1615	-0.1615	-0.1615	0.0686	0.0686	0.0686	0.0686	0.0686
STO_T_251469324932	0.0305	0.0343	0.0343	0.0343	0.0343	0.0343	0.1206	0.1206	0.1206	0.1206	0.1206
STO_T_251469325960	-0.0308	0.0064	0.0064	0.0064	0.0064	0.0064	-0.1043	-0.1043	-0.1043	-0.1043	-0.1043
STO_T_251469325957	-0.1673	0.2297	0.2297	0.2297	0.2297	0.2297	0.1694	0.1694	0.1694	0.1694	0.1694
STO_T_251469320890	-0.2825	-0.0743	-0.0743	-0.0743	-0.0743	-0.0743	-0.2068	-0.2068	-0.2068	-0.2068	-0.2068
STO_T_251469324946	-0.0075	-0.0748	-0.0748	-0.0748	-0.0748	-0.0748	-0.2133	-0.2133	-0.2133	-0.2133	-0.2133
STO_T_251469325959	-0.0164	-0.1547	-0.1547	-0.1547	-0.1547	-0.1547	-0.1523	-0.1523	-0.1523	-0.1523	-0.1523
STO_T_251469324947	0.0103	-0.0175	-0.0175	-0.0175	-0.0175	-0.0175	1.2835	1.2835	1.2835	1.2835	1.2835
STO_T_251469325958	-0.0585	0.0148	0.0148	0.0148	0.0148	0.0148	-0.3543	-0.3543	-0.3543	-0.3543	-0.3543
STO_T_251469320946	0.0238	0.0029	0.0029	0.0029	0.0029	0.0029	-0.577	-0.577	-0.577	-0.577	-0.577
STO_T_251469325961	-0.2128	0.1303	0.1303	0.1303	0.1303	0.1303	-0.1349	-0.1349	-0.1349	-0.1349	-0.1349
STO_T_251469324948	0.0449	0.0064	0.0064	0.0064	0.0064	0.0064	0.0409	0.0409	0.0409	0.0409	0.0409
STO_T_251469324933	-0.057	-0.0963	-0.0963	-0.0963	-0.0963	-0.0963	0.0091	0.0091	0.0091	0.0091	0.0091
STO_T_251469320396	-0.0349	-0.0348	-0.0348	-0.0348	-0.0348	-0.0348	-0.0094	-0.0094	-0.0094	-0.0094	-0.0094
STO_T_251469320393	0.0784	-0.0836	-0.0836	-0.0836	-0.0836	-0.0836	-0.1634	-0.1634	-0.1634	-0.1634	-0.1634
STO_T_251469320935	0.0332	0.1229	0.1229	0.1229	0.1229	0.1229	-0.0013	-0.0013	-0.5015	-0.5015	-0.5015
STO_T_251469320840	0.0263	0.076	0.076	0.076	0.076	0.076	-0.1169	-0.1169	-0.1169	-0.1169	-0.1169
STO_T_251469320842	-0.0199	-0.0374	-0.0374	-0.0374	-0.0374	-0.0374	-0.1643	-0.1643	-0.1643	-0.1643	-0.1643

STO_T_251469320949	0.0477	0.1236	0.1236	0.1236	0.1236	0.1236	-0.0884	-0.0884	-0.0884	-0.0884	-0.0884
STO_T_251469320846	-0.0704	-0.1128	-0.1128	-0.1128	-0.1128	-0.1128	-0.1722	-0.1722	-0.1722	-0.1722	-0.1722
STO_T_251469320394	-0.0828	0.1863	0.1863	0.1863	0.1863	0.1863	0.0019	0.0019	0.0019	0.0019	0.0019
STO_T_251469320395	-0.0131	0.0473	0.0473	0.0473	0.0473	0.0473	0.0307	0.0307	0.0307	0.0307	0.0307
STO_T_251469320375	-0.1403	0.081	0.081	0.081	0.081	0.081	-0.1617	-0.1617	-0.1617	-0.1617	-0.1617
STO_T_251469320948	-0.1295	-0.1539	-0.1539	-0.1539	-0.1539	-0.1539	-0.0803	-0.0803	-0.0803	-0.0803	-0.0803
STO_T_251469320947	0.2737	0.1339	-0.1539	-0.1539	-0.1539	-0.1539	0.1543	0.1543	0.1543	0.1543	0.1543
STO_T_251469320839	-0.1433	-0.0161	-0.0161	-0.0161	-0.0161	-0.0161	0.1972	0.1972	0.1972	0.1972	0.1972
STO_T_251469320971	-0.0051	-0.1338	-0.1338	-0.1338	-0.1338	-0.1338	-0.0918	-0.0918	-0.0918	-0.0918	-0.0918
STO_T_251469324922	-0.1378	0.0674	0.0674	0.0674	0.0674	0.0674	-0.2242	-0.2242	-0.2242	-0.2242	-0.2242
STO_T_251469320463	0.0668	0.1339	-0.0588	-0.0588	-0.0588	-0.0588	-0.2692	-0.2692	-0.2692	-0.2692	-0.2692
STO_T_251469320450	-0.0419	0.0472	0.0472	0.0472	0.0472	0.0472	-0.4708	-0.4708	-0.4708	-0.4708	-0.4708
STO_T_251469320464	0.0439	0.0416	0.0416	0.0416	0.0416	0.0416	0.0466	0.0466	0.0466	0.0466	0.0466
STO_T_251469320378	0.0265	0.0151	-0.0912	-0.0912	-0.0912	-0.0912	-0.3419	-0.3419	-0.3419	-0.3419	-0.3419
STO_T_251469320376	0.006	0.0164	0.0164	0.0164	0.0164	0.0164	0.0209	0.0209	0.0209	0.0209	0.0209
STO_T_251469320377	0.2063	-0.0808	-0.0808	-0.0808	-0.0808	-0.0808	-0.0866	-0.0866	-0.0866	-0.0866	-0.0866
STO_T_251469320380	-0.0528	0.6458	0.6458	0.6458	0.6458	0.6458	-0.1636	-0.1636	-0.1636	-0.1636	-0.1636
STO_T_251469324923	0.1634	0.0045	0.0045	0.0045	0.0045	0.0045	0.1171	0.1171	0.1171	0.1171	0.1171
STO_T_251469320465	0.0808	0.0538	0.0538	0.0538	0.0538	0.0538	0.1467	0.1467	0.1467	0.1467	0.1467
STO_T_251469320451	0.0261	0.0179	0.0179	0.0179	0.0179	0.0179	0.0602	0.0602	0.0602	0.0602	0.0602
STO_T_251469320379	-0.0075	-0.0114	-0.0114	-0.0114	-0.0114	-0.0114	-0.0761	-0.0761	-0.0761	-0.0761	-0.0761
STO_T_251469326311	-0.0948	-0.2009	-0.2009	-0.2009	-0.2009	-0.2009	-0.038	-0.038	-0.038	-0.038	-0.038
STO_T_251469326310	-0.0422	-0.2003	-0.2003	-0.2003	-0.2003	-0.2003	-0.0462	-0.2795	-0.2795	-0.2795	-0.2795
STO_HKN-7_251469320927	-0.4777	-0.4255	-0.4255	-0.4255	-0.4255	-0.4255	-0.2561	-0.2561	-0.2561	-0.2561	-0.2561
STO_HS-746T_251469320945	0.0668	-0.3632	-0.3632	-0.3632	-0.3632	-0.3632	0.0234	0.0234	0.0234	0.0234	0.0234
STO_IM-95_251469320942	-0.0324	-0.331	-0.331	-0.331	-0.331	-0.331	-0.0102	-0.0102	-0.0102	-0.0102	-0.0102
STO_SNU-1_251469320944	-0.012	0.1175	0.1175	0.1175	0.1175	0.1175	0.0134	0.0134	0.0134	0.0134	0.0134
STO_SNU-16_251469320943	-0.1124	0.0239	0.0239	0.0239	0.0239	0.0239	-0.6776	-0.6776	-0.6776	-0.6776	-0.6776
STO_SNU-5_251469320941	0.0525	0.1372	0.1372	0.1372	0.1372	0.1372	-0.134	-0.134	-0.134	-0.134	-0.134
STO_YCC-7_251469313194	-0.3658	-0.0357	-0.0357	-0.0357	-0.0357	-0.0357	-0.4278	-0.4278	-0.4278	-0.4278	-0.4278
STO_YCC-6_251469313195	0.3955	-0.157	-0.157	-0.157	-0.157	-0.157	-0.4956	-0.4956	-0.4956	-0.4956	-0.4956
STO_YCC-1_251469320903	-0.2705	0.41	0.41	0.41	0.41	0.41	0.0928	0.0928	0.0928	0.0928	0.0928
STO_YCC-16_251469320904	0.4385	0.1902	0.1902	0.1902	0.1902	0.1902	-1.1595	-1.1595	-1.1595	-1.1595	-1.1595
STO_KATO-111_25146932090	0.0594	-0.1767	-0.1767	-0.1767	-0.1767	-0.1767	0.1362	0.1362	0.1362	0.1362	0.1362
STO_YCC-11_251469320906	-0.0151	0.1786	0.1786	0.1786	0.1786	0.1786	0.0616	0.0616	0.0616	0.0616	0.0616
STO_YCC-2_251469320928	-0.1268	0.0025	0.0025	0.0025	0.0025	0.0025	-0.2216	-0.2216	-0.2216	-0.2216	-0.2216
STO_FU-97_251469320929	0.3241	-0.1411	-0.1411	-0.1411	-0.1411	-0.1411	-0.5512	-0.5512	-0.5512	-0.5512	-0.5512
STO_YCC-9_251469320930	0.1437	-0.2176	-0.2176	-0.2176	-0.2176	-0.2176	-0.5211	-0.5211	-0.5211	-0.5211	-0.5211
STO_N-87_251469320931	0.1234	0.03	0.03	-0.1877	-0.1877	-0.1877	-0.7295	-0.7295	-0.7295	-0.7295	-0.7295
STO_AGS-_251469312769	-0.0836	0.097	0.097	0.097	0.097	0.097	-0.1008	-0.1008	-0.1008	-0.1008	-0.1008
STO_X_251469326125	-0.0088	-0.0247	-0.0247	-0.0247	-0.0247	-0.0247	-0.1988	-0.1988	-0.1988	-0.1988	-0.1988
STO_X_251469326126	-0.0406	-0.0445	-0.0445	-0.0445	-0.0445	-0.0445	0.2648	0.2648	0.2648	0.2648	0.2648
STO_X_251469326127	-0.1448	0.1539	0.1539	0.1539	0.1539	0.1539	-0.1736	-0.1736	-0.1736	-0.1736	-0.1736
STO_X_251469326128	-0.8625	0.0418	0.0418	0.0418	0.0418	0.0418	-0.0035	-0.0035	-0.0035	-0.0035	-0.0035
STO_X_251469324560	0.0497	-0.26	-0.26	-0.26	-0.26	-0.26	0.056	0.056	0.056	0.056	0.056
STO_X_251469331100	0.0338	0.1375	0.1375	0.1375	0.1375	0.1375	-0.2695	-0.2695	-0.2695	-0.2695	-0.2695
STO_X_251469331645	-0.08	0.0312	0.0312	0.0312	0.0312	0.0312	-0.0902	-0.0902	-0.0902	-0.0902	-0.0902
STO_X_251469331058	-0.0469	0.0113	0.0113	0.0113	0.0113	0.0113	-0.0112	-0.0112	-0.0112	-0.0112	-0.0112
STO_A2521-R_251469320385	-0.0122	0.0706	0.0706	0.0706	0.0706	0.0706	0.0541	0.0541	0.0541	0.0541	0.0541
STO_MKN28R_251469320383	-0.0491	-0.1496	-0.1496	-0.1496	-0.1496	-0.1496	-0.6033	-0.6033	-0.6033	-0.6033	-0.6033
STO_MKN1-R_251469320381	0.2219	-0.1536	-0.1536	-0.1536	-0.1536	-0.1536	-1.232	-1.232	-1.232	-1.232	-1.232
STO_MKN45-R_251469326216	1.1811	-0.1314	-0.1314	-0.1314	-0.1314	-0.1314	-1.0949	-1.0949	-1.0949	-1.0949	-1.0949
STO_TMK1-R_251469320382	0.0712	-0.2825	-0.2825	-0.2825	-0.2825	-0.2825	-0.1682	-0.1682	-0.1682	-0.1682	-0.1682
STO_YCC10R_251469326215	-0.0102	-0.2678	-0.2678	-0.2678	-0.2678	-0.2678	0.0477	0.0477	-0.0978	-0.0978	-0.0978
STO_YCC7KDR_25146932038	-0.5406	-0.1	-0.1	-0.1	-0.1	-0.1	-0.4504	-0.4504	-0.4504	-0.4504	-0.4504
STO_YCC-7-R_251469326214	-0.388	-0.1995	-0.1995	-0.1995	-0.1995	-0.1995	-0.4643	-0.4643	-0.4643	-0.4643	-0.4643
STO_X_251469326217	-0.0591	-0.0519	-0.0519	-0.0519	-0.0519	-0.0519	0.2552	0.2552	0.2552	0.2552	0.2552
STO_X_251469324561	-0.0622	-0.0299	-0.0299	-0.0299	-0.0299	-0.0299	0.0179	0.0179	0.0179	0.0179	0.0179

STO_X_251469324562	0.1262	-0.0475	-0.0475	-0.0475	-0.0475	-0.0475	0.1251	0.1251	0.1251	0.1251	0.1251
STO_X_251469324563	-0.0679	-0.0345	-0.0345	-0.0345	-0.0345	-0.0345	-0.0804	-0.0804	-0.0804	-0.0804	-0.0804
STO_X_251469324565	-0.0768	-0.0498	-0.0498	-0.0498	-0.0498	-0.0498	0.063	0.063	0.063	0.063	0.063
STO_X_251469331073	-0.2282	0.0441	0.0441	0.0441	0.0441	0.0441	-0.1277	-0.1277	-0.1277	-0.1277	-0.1277
STO_X_251469331074	-0.3565	0.2361	0.2361	0.2361	0.2361	0.2361	-0.0897	-0.0897	-0.0897	-0.0897	-0.0897
STO_X_251469331057	-0.1617	-0.0355	-0.0355	-0.0355	-0.0355	-0.0355	-0.375	-0.375	-0.375	-0.375	-0.375
STO_X_251469331098	-0.6441	0.1184	0.1184	0.1184	0.1184	0.1184	0.0796	0.0796	0.0796	0.0796	0.0796
STO_X_251469331102	0.0105	0.0799	0.0799	0.0799	0.0799	0.0799	0.0421	0.0421	0.0421	0.0421	0.0421
STO_X_251469331644	0.0545	-0.006	-0.006	-0.006	-0.006	-0.006	-0.0604	-0.0604	-0.0604	-0.0604	-0.0604
STO_X_251469331059	-0.2245	-0.085	-0.085	-0.085	-0.085	-0.085	-0.2775	-0.2775	-0.2775	-0.2775	-0.2775
STO_X_251469331101	-0.058	-0.1355	-0.1355	-0.1355	-0.1355	-0.1355	0.2648	0.2648	0.2648	0.2648	0.2648
STO_X_251469331646	0.0589	0.0902	0.0902	0.0902	0.0902	0.0902	0.0223	0.0223	0.0223	0.0223	0.0223
STO_X_251469331099	-0.1373	0.0663	0.0663	0.0663	0.0663	0.0663	-0.5789	-0.5789	-0.5789	-0.5789	-0.5789
STO_X_251469331643	-0.0606	-0.0295	-0.0295	-0.0295	-0.0295	-0.0295	0.0883	0.0883	0.0883	0.0883	0.0883
STO_X_251469331642	0.0027	-0.0057	-0.0057	-0.0057	-0.0057	-0.0057	-0.0272	-0.0272	-0.0272	-0.0272	-0.0272
STO_X_251469311580	-0.0186	0.1573	0.1573	0.1573	0.1573	0.1573	-0.0169	-0.0169	-0.0169	-0.0169	-0.0169
STO_X_251469311579	-0.0876	0.0016	0.0016	0.0016	0.0016	0.0016	-0.0242	-0.0242	-0.0242	-0.0242	-0.0242
STO_X_251469311578	0.0895	0.0154	0.0154	0.0154	0.0154	0.0154	-0.2159	-0.2159	-0.2159	-0.2159	-0.2159
STO_X_251469326218	0.0143	-0.0291	-0.0291	-0.0291	-0.0291	-0.0291	0.0576	0.0576	0.0576	0.0576	0.0576
STO_X_251469326124	-0.0789	0.0938	0.0938	0.0938	0.0938	0.0938	0.2681	0.2681	0.2681	0.2681	0.2681

*Column B to L represents log 2 transformed Relative probe intensity compared to normal

Supplementary References

1. B. P. Lewis, I. H. Shih, M. W. Jones-Rhoades, D. P. Bartel, C. B. Burge, *Cell* **115**, 787 (Dec 26, 2003).
2. A. Krek *et al.*, *Nat Genet* **37**, 495 (May, 2005).
3. B. John *et al.*, *PLoS Biol* **2**, e363 (Nov, 2004).
4. V. Rusinov, V. Baev, I. N. Minkov, M. Tabler, *Nucleic Acids Res* **33**, W696 (Jul 1, 2005).
5. S. A. Tomlins *et al.*, *Science* **310**, 644 (Oct 28, 2005).
6. S. A. Tomlins *et al.*, *Nature* **448**, 595 (Aug 2, 2007).
7. S. Varambally *et al.*, *Nature* **419**, 624 (2002).
8. I. D. Ferreira, V. E. Rosario, P. V. Cravo, *Malar J* **5**, 1 (2006).
9. S. G. Malakho, A. Korshunov, A. M. Stroganova, A. B. Poltaraus, *J Clin Lab Anal* **22**, 123 (2008).
10. C. G. Mullighan *et al.*, *Nature* **446**, 758 (Apr 12, 2007).
11. X. Zhao *et al.*, *Cancer Res* **65**, 5561 (Jul 1, 2005).
12. A. B. Olshen, E. S. Venkatraman, R. Lucito, M. Wigler, *Biostatistics* **5**, 557 (Oct, 2004).
13. C. G. Kleer *et al.*, *Proc Natl Acad Sci U S A* **100**, 11606 (Sep 30, 2003).
14. K. Collett *et al.*, *Clin Cancer Res* **12**, 1168 (Feb 15, 2006).
15. R. H. Breuer *et al.*, *Neoplasia* **6**, 736 (Nov-Dec, 2004).
16. T. Sudo *et al.*, *Br J Cancer* **92**, 1754 (May 9, 2005).
17. S. Weikert *et al.*, *Int J Mol Med* **16**, 349 (Aug, 2005).
18. A. P. Bracken *et al.*, *EMBO J* **22**, 5323 (Oct 15, 2003).
19. I. M. Bachmann *et al.*, *J Clin Oncol* **24**, 268 (Jan 10, 2006).